Determination of Thallium and Indium with an Electrochemically-reduced Graphene Oxide-Carbon Paste Electrode by Anodic Stripping Voltammetry

A thesis submitted in fulfilment of the requirements for the degree of

Magister Scientiae in Nanoscience (Chemistry)

Department of Chemistry: Sensor Lab

University of Western Cape

Supervisor: Prof N. Jahed

Co-supervisor: Prof E.I. Iwuoha

by

Tayla Martin

3.5 Square wave analysis

Square wave analysis was performed using a 797 VA COMPUTRACE instrument (Metrohm, Switzerland) controlled by a personal computer. A three electrochemical system consisting of an electrodeposited graphene oxide carbon paste electrode (ERGO-CPE) served as the working electrode. An Ag/AgCl (saturated KCl) and platinum wire served as the reference and counter electrode, respectively. All experiments were performed in a one compartment 20 mL voltametric cell at room temperature.

The cell, Teflon stirrer, counter electrode and reference electrode were cleaned with ethanol and rinsed with distilled water. 0.1 M acetate buffer (20ml) was pipetted into the voltammetric cell. The voltammogram was recorded by applying a potential from -1.5 to 0.3 V using SWASV with rotating speed (1000 rpm), voltage step (0.005 V) and frequency (50 Hz), deposition time (120 s) and amplitude (0.02 V).

The optimum instrumental parameters were determined by changing one and keeping the remaining ones constant. The effect of the peak heights produced by the current were investigated.

A bare carbon paste electrode submerged in only buffer solution was placed in the cell and a baseline was recorded. This was done to determine if the surface of the electrode was clean and if any contamination is present.

Table 3. 1: Chemical reagents used in this work

Chemicals	Source
Graphite powder	Sigma-Aldrich
Mineral oil	Sigma-Aldrich
Potassium permanganate ($KMnO_4$)	PAL Chemicals
98% Sulfuric acid (H_2SO_4)	KIMIX
85% Phosphoric acid	KIMIX
Hydrogen peroxide (H_2O_2)	Sigma-Aldrich
32% Hydrochloric acid (HCl)	KIMIX
99.9% Ethanol (CH_2CH_3OH)	KIMIX
Sodium acetate	Sigma-Aldrich
Acetic acid	Sigma-Aldrich
Thallium	Sigma-Aldrich
Indium	Sigma-Aldrich

3.6 Preparation of Graphene oxide

Preparation of graphene oxide was prepared by the modified Hummer's method. Graphite powder (3 g) was mixed with potassium permanganate (18g). Concentrated sulfuric acid (360 ml) was added to phosphoric acid (40 ml). The concentrated acids were added slowly to the powder mixture. As the mixture was stirred the temperature increased, due to an exothermic reaction. A heater stirrer was used at 50^{o}C with a magnetic stirrer for 12 hours.

After 12 hours, the mixture was cooled down to room temperature. It was poured over deionized ice water (400 ml). An excess of hydrogen peroxide was added with a pipette until a bright yellow colour was obtained. The liquid was poured into measuring tubes and centrifuged for 15 minutes. After centrifuging the liquid was decanted and washed with 10%

HCl and ultra-pure water until the precipitant was basic. It was then dried in a vacuum oven at 70^{o}C for 48 hours. Graphene oxide was grinded into powder using a mortar and pestle.

3.7 Preparation of electrochemical reduced Graphene oxide to form electricochemically-reduced Graphene oxide carbon paste electrodes (ERGO-CPE)

The cyclic voltammetric reduction was performed in 20 ml of GO dispersion (1 mg mL^{-1}) on a 797 VA Computrace instrument in the potential range between -1.4 to +0.3 V for 10 cycles. The instrumental parameters were: deposition time (30 s), deposition potential (-1.4 V), frequency (50 Hz), amplitude (0.02 V) and voltage step (0.005 V).

3.8 Preparation of carbon paste electrodes

Graphite powder (0.5 g) was mixed with mineral oil (182 µL) in a mortar and pestle for 30 minutes until homogenous paste is obtained. The paste was packed in the carbon paste body cavity. The electrode was polished on weighing paper until the excess was removed.

3.9 Characterization techniques

a) Scanning Electron Microscopy

Scanning Electron Microscopy (SEM) measurements were performed using an Auriga SEM 30 kV instrument equipped with Electronic Data System (EDS) and images were taken using the secondary electron detector. The samples were prepared on an aluminium stub which was coated with either Carbon or Iridium.

b) High resolution transmission electron microscopy

High Resolution Transmission Electron Microscopy (HRTEM) measurements were carried out with a Tecnai G2 F20X-Twin MAT Field Emission Transmission Electron Microscope from FEI (Eindhoven, Netherlands) under an acceleration voltage of 200 kV. The samples were prepared by dropping a dilute suspension of graphite or graphene oxide in ethanol onto copper grids followed by air drying at room temperature.

c) Fourier transformed infrared (FT-IR) spectroscopy

A Fourier Transform Infrared (FT-IR) spectrum was recorded using a (Perkin Elmer Spectrum 100) coupled to an Attenuated Total Reflectance (ATR) sample holder. FT-IR was used to obtain information and confirmation on graphite or graphene oxide in the range 4000-1000 cm^{-1}.

d) X-ray diffraction (XRD)

XRD was used to analyse the phase purity and crystalline nature of the graphene oxide [71]. XRD measurements were carried out using a Bruker AXS D8 Advance diffractometer from BRUKER- AXS Germany with Cu-Kα radiation.

e) Raman spectroscopy

Raman and Fourier Transform Infrared Spectroscopy are used to detect vibrations in molecules. They provide information on chemical structures and physical forms to identify substances which is unique to the species being studied [72]. Raman spectroscopy was obtained using a Dilor XY Raman spectrometer with a Coherent Innova 300 Argon laser. Graphite and Graphene oxide was excited with a 514.5 nm laser to enable wavelength absorption. Adhesive glue was used to hold the sample onto the glass slide and then placed onto the stage of the Raman instrument for analysis.

Chapter Four:

Morphology and structural characterization of graphene oxide

4.1 Introduction

This chapter describes and explains the morphological and structural changes of Graphene oxide. HR-SEM, HR-TEM, XRD, FTIR and Raman Spectroscopy were used to confirm the formation of multi-layer graphene oxide sheets to be used as a sensing platform for the detection of Thallium and Indium by Anodic Stripping Voltammetry.

4.2 High-Resolution Scanning electron microscope (HR-SEM)

Scanning electron microscope provides morphology and structure of nanomaterials. The samples prepared for SEM analysis was placed on an aluminium stub and coated with Iridium or Carbon. The HR-SEM images of high grade commercial Graphite and Graphene oxide synthesized by the modified Hummer's method [73] are shown in Figure 4.1 (a and b) and (c and d), respectively. Thin paper-like sheets of Graphite was shown in Figure 4.1 (a and b) at low and high magnification. At higher magnification, the straight, sharp edges of graphite owe to its highly ordered crystalline orientation [13, 73]. From the SEM image in Figure 4.1 (c and d) it's clearly visible that GO has a multiple lamellar layer and the films are stacked one above the other [59]. At a higher magnification in Figure 4.1d , the surface of GO is uneven due to oxidation of sheets [74].

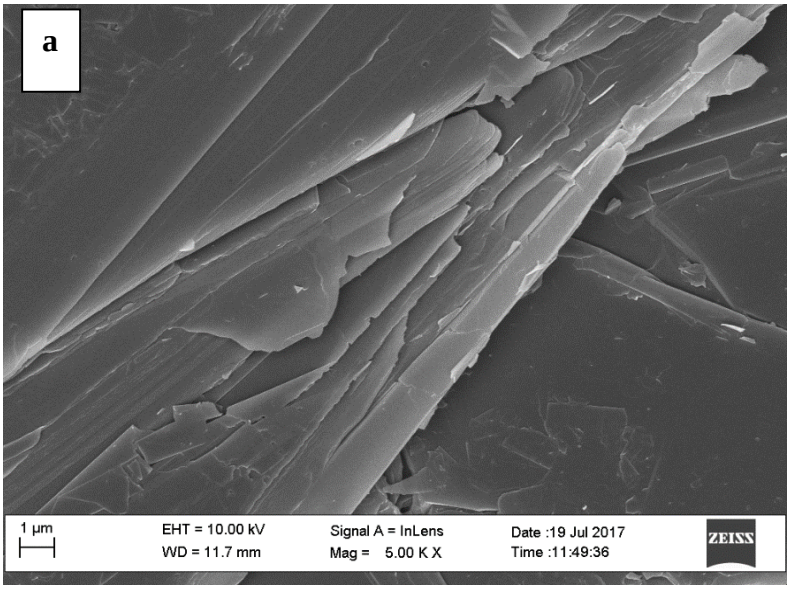

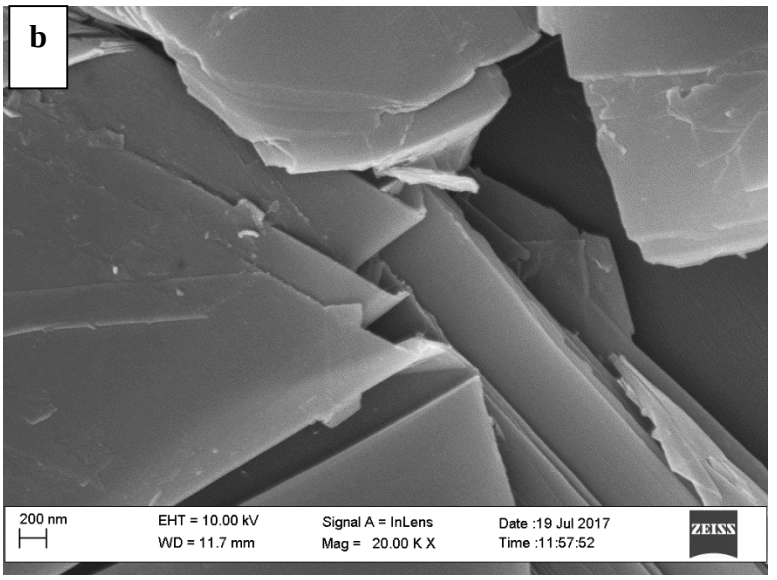

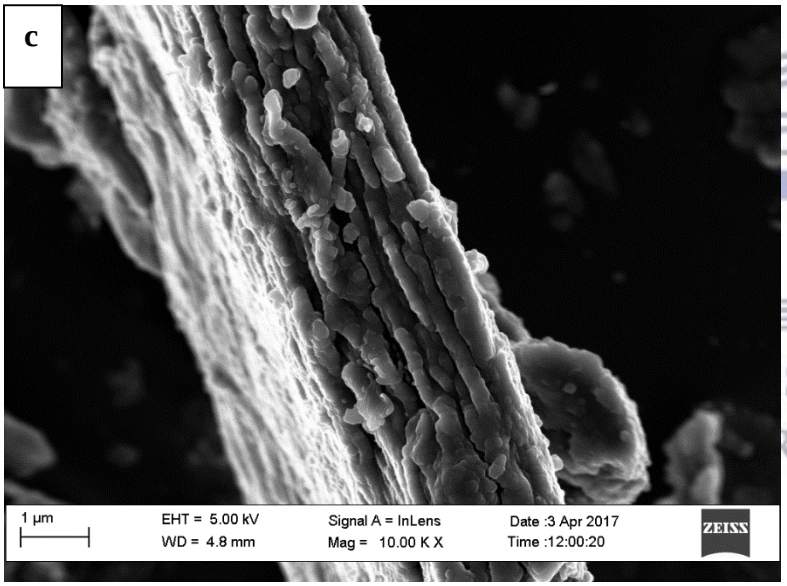

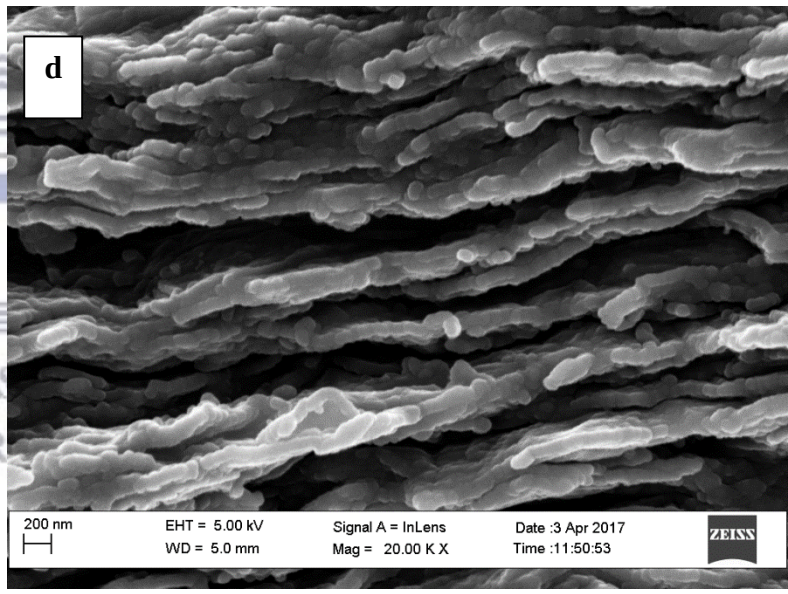

Figure 4. 1: HR-SEM images of (a and b) Graphite and (c and d) Graphene oxide

4.3 High-Resolution Transmission Electron Microscope

Graphite and Graphene oxide samples were prepared by suspension in ethanol, sonicated and then drop casted onto a Cu grid. The surface morphology and crystalline nature of Graphite and Graphene oxide was analysed by HR-TEM in Figure 4.2 (a-d) [71]. In Figure 4.2a straight edges of pure graphite was revealed which suggested a highly ordered crystalline orientation [13]. At higher magnification in Figure 4.2b, the larger and increasingly transparent sheets in graphite resemble wavy silk veils entangled with one another [13]. In Figure 4.2c the edges of GO are thicker due to the oxygen-containing groups [59]. An increase in transparency at higher magnification suggests regions of single layer GO sheets in Figure 4.2d [75].

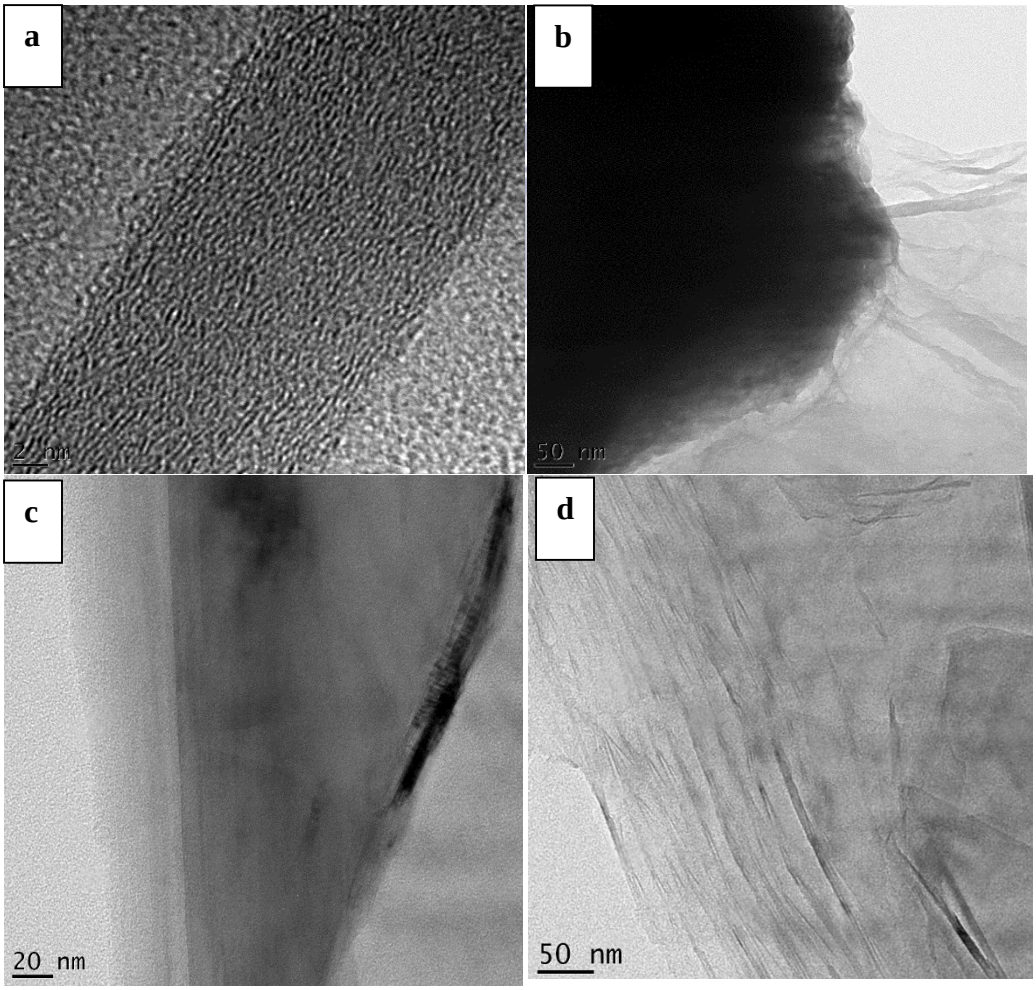

Figure 4. 2: HR-TEM images of (a and b) Graphite and (c and d) Graphene oxide

4.4 X-ray diffraction

X-ray Diffraction (XRD) was used to determine the phase formation and crystallinity [64] of Graphite and Graphene oxide [71]. X-ray diffraction images of Graphite and Graphene oxide are shown in Figure 4.3 (a and b), respectively. The strong, distinct peak at 26.56° as 002 in Figure 4.3a with an inter-planar distance of 0.34 nm using Braggs law indicates a highly ordered carbon structure. The peak indexed as 100 at 43.10° indicates the crystalline structure of graphite [13]. In Figure 4.3b, the appearance of the peak as 001 at 10° results in complete oxidation after chemical oxidation [61] and exfoliation, which indicate an increase in d-spacing from 0.34 nm to 0.82 nm and also [71] due to interlayer spacing which confirms the presence of oxygen functional groups [13, 71]. The broad peak as 002 at 26° indicate an increased disorder, structural defects due to sonication and exfoliated sheets [74, 59]. Similar results are reported in Marcano *et al.* [73].

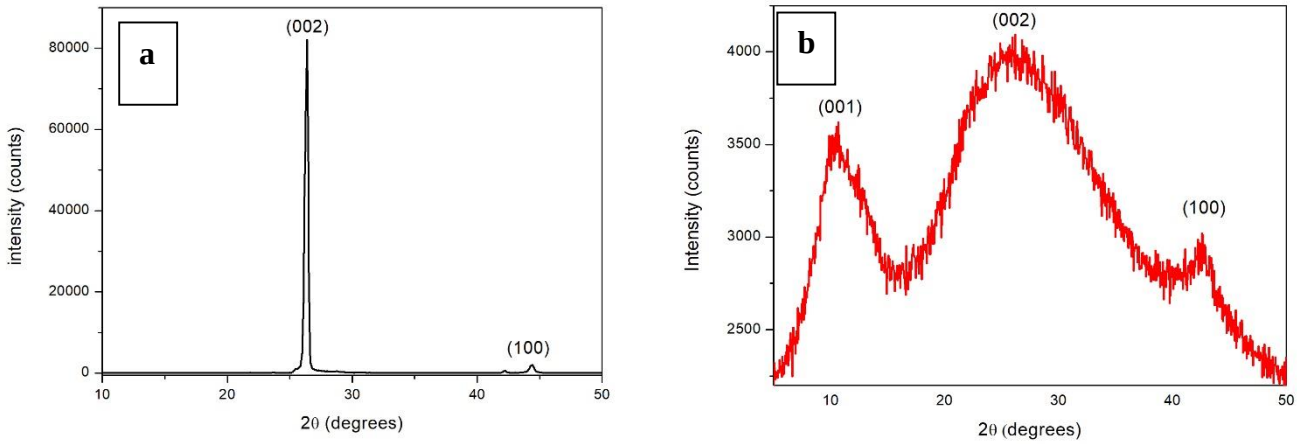

Figure 4. 3: XRD of (a) Graphite and (b) Graphene oxide

4.5 Fourier Transform Infrared Spectroscopy

FTIR analysis was done in order to investigate the structure and functional groups in pure Graphite and Graphene oxide. In Figure 4.4a, pure Graphite revealed no significant functional groups whereas in Figure 4.4b, the broad peak at 3400 cm^{-1} was due to the O-H group present in GO due to the adsorbed water molecules [61] which indicated strong hydrophilicity [73], the carboxyl C=O group appeared at 1720 cm^{-1} due to the edges of GO sheets [71, 76], aromatic C=C groups are present at 1620 cm^{-1} confirms the oxidation of graphite [76]. The stretching vibration of C-O was present at 1050 cm^{-1} which resulted in the oxide functional groups after the oxidation process [61, 69].

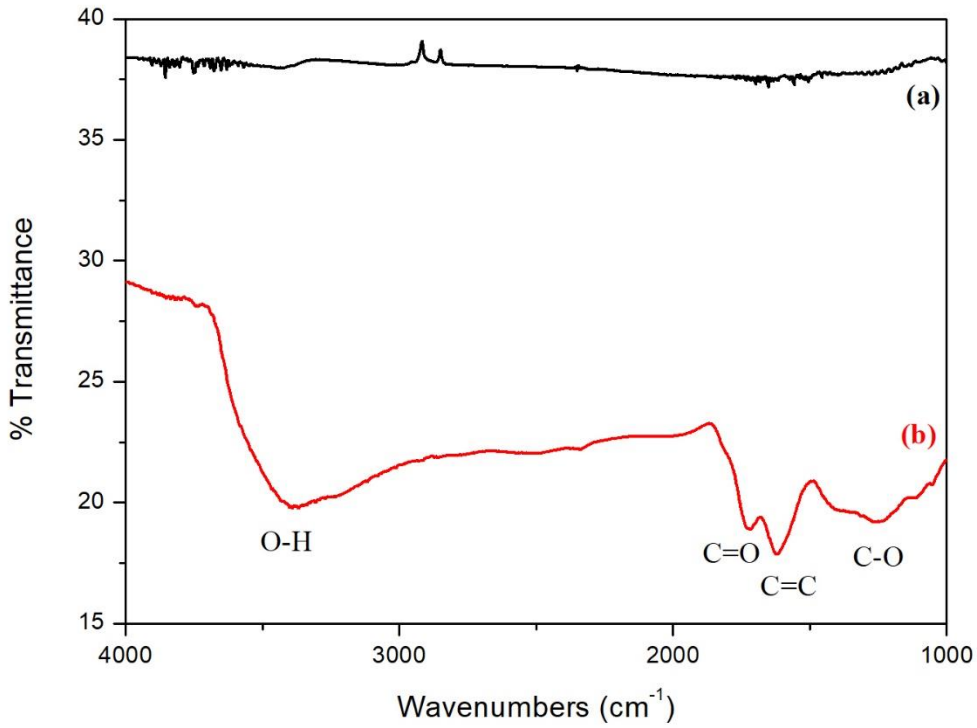

Figure 4. 4: FT-IR spectra of (a) Graphite and (b) Graphene oxide

4.6 Raman Spectroscopy

The change in structure and exfoliation behaviour from graphite to graphene oxide was investigated by Raman spectroscopy and presented by Figure 4.5 (a and b), respectively. The Raman spectra of graphite is shown in Figure 4.5a. The Raman spectra for graphite revealed a sharp G band at 1575 cm^{-1} due to first order scattering of the E_2g mode [56 71] and a significantly weaker D band at 1350 cm^{-1} . The D band is evident for the presence of defects in the graphite material such as bond-angle disorder, bond-length order, vacancies and edge defects [71, 13, 56]. The ratio of the intensities of the D and G bands (I_D/I_G), used as a measure of disorder was calculated as 0.089. The Raman spectra of graphene oxide is shown in Figure 4.5b, showed the D peak located at 1360 cm^{-1} and G peak at 1600 cm^{-1}. The G peak attributes to the in-phase vibration of the sp^2 carbons while the D peak obtained is due to the crystal disorder [56 61, 67]. The calculated I_D/I_G ratio obtained was 0.84, which resulted in an increase in structural disorder [74].

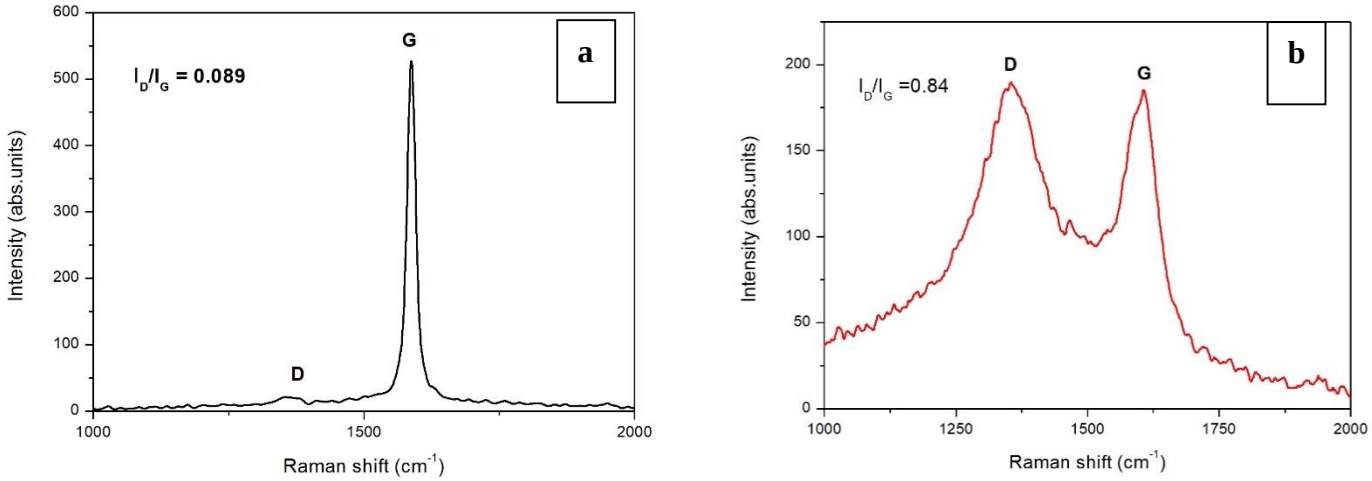

Figure 4. 5: Raman spectrum of (a) Graphite and (b) Graphene oxide

Chapter Five:

Electrochemically-reduced Graphene oxide Carbon Paste Electrodes (ERGO-CPE)

5.1 Introduction

In this chapter an electrochemical reduction technique was used to prepare electrochemically reduced graphene oxide modified carbon paste electrode from graphene oxide solutions. The modified carbon paste electrodes were applied for the determination of TI^{1+} and In^{3+} by Anodic Stripping Voltammetry.

5.2 Electrochemical reduction of graphene oxide

Electrochemically reduced graphene oxide thin films were produced on the carbon paste electrode surface by a direct electrochemical reduction of GO sheets from an aqueous colloidal suspension in acetate buffer solution [13]. Cyclic voltammograms obtained from the electrochemical reduction of a graphene oxide solution (1 mg mL^{-1}) onto CPEs are depicted in Figure 5.1. The cyclic voltammogram show an anodic peak (I) and cathodic peak (II). The redox couple (I and II) confirmed the deposition ERGO on the CPE surface [74]. An increase in anodic peak (I) at 0.2 V with increasing number of scans was observed while the cathodic peak (II) at -0.6 V increases until the fourth cycle then stabilized. The redox behaviour can be appointed to the deposition of ERGO sheets that are formed by the reduction of graphene oxide onto the surface of the electrode [13].

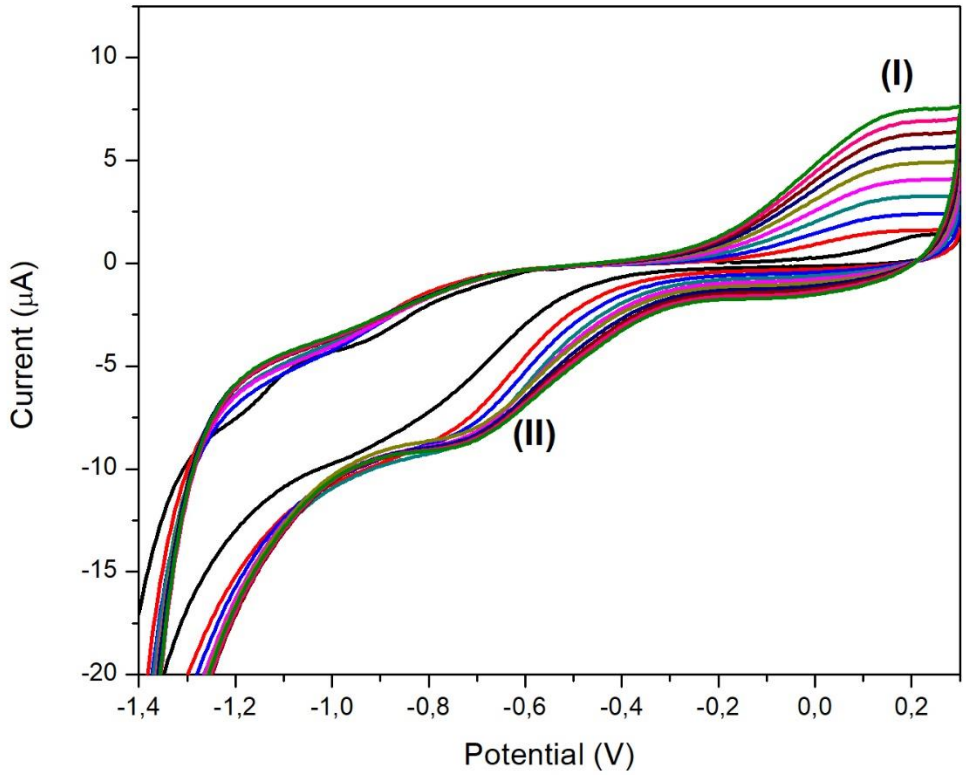

Figure 5. 1: Cyclic voltammograms depicting the electrochemical reduction of 1 mg mL^{-1} GO in acetate buffer solution (0.1 M, pH 4.6) at the CPE at the following instrumental parameters: scan rate (100 mVs^{-1}), deposition time (30 s), frequency (50 Hz), deposition potential (-1.4 V) and voltage step (0.005)

5.3 Electrochemical characterization of the modified carbon paste electrode

Cyclic voltammograms for the unmodified CPE and ERGO-CPE recorded in 0.1 M acetate buffer solution are shown in Figure 5.2. The larger background current of ERGO-CPE compared to the unmodified CPE confirmed the enhanced electronic conductivity and electron transfer of reduced graphene oxide when immobilized at the electrode surface [13].

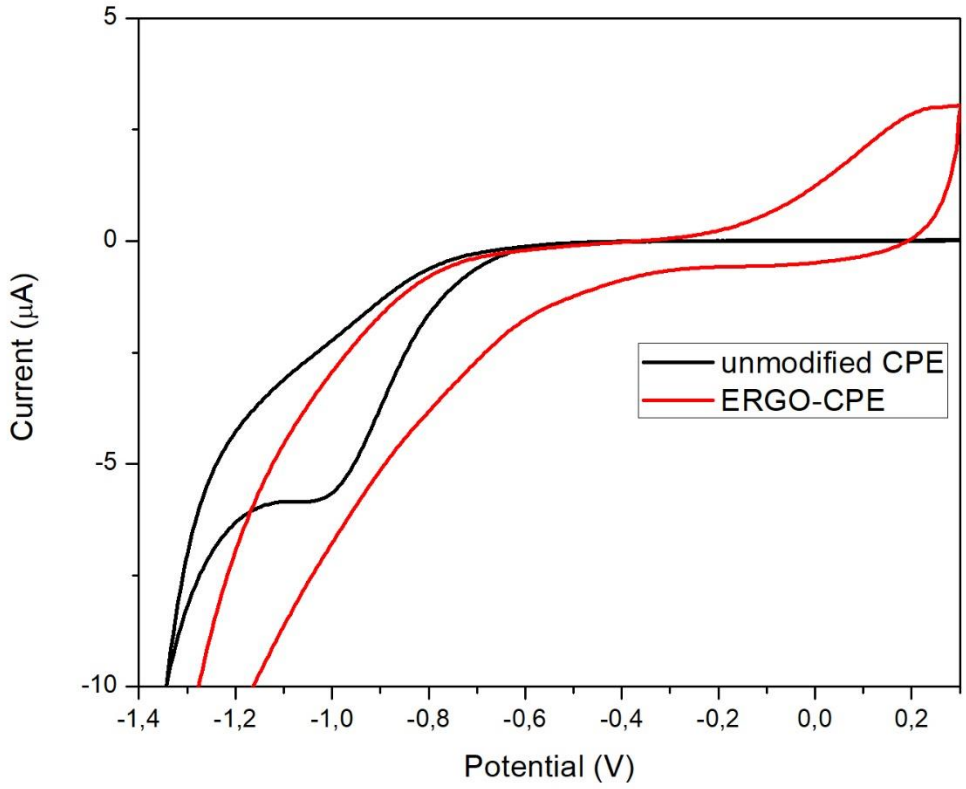

Figure 5. 2: Cyclic voltammograms of unmodified CPE and ERGO-CPE in acetate buffer solution (0.1 M, pH 4.6) at the following instrumental parameters: scan rate (100 mVs^{-1}), deposition time (30 s), frequency (50 Hz), deposition potential (-1.4 V) and voltage step (0.005 V)

5.4 Influence of the number of electrodeposition cycles

The speed and ease of electron transfer through a film is significantly important to the performance and sensitivity of any working electrode [13]. Figure 5.3 showed that the number of electrochemical reduction cycles influenced the stripping peak currents of TI^{1+} and In^{3+}. A general increase in peak currents is observed for TI^{1+} up to 10 cycles, whereas an increase at 15 cycles for In^{3+} was observed. A deposition of ten cycles was selected for TI^{1+} and In^{3+} at ERGO-CPE after which, the thickness of graphene oxide film hinders the flow of electrons to the electrode surface [13].

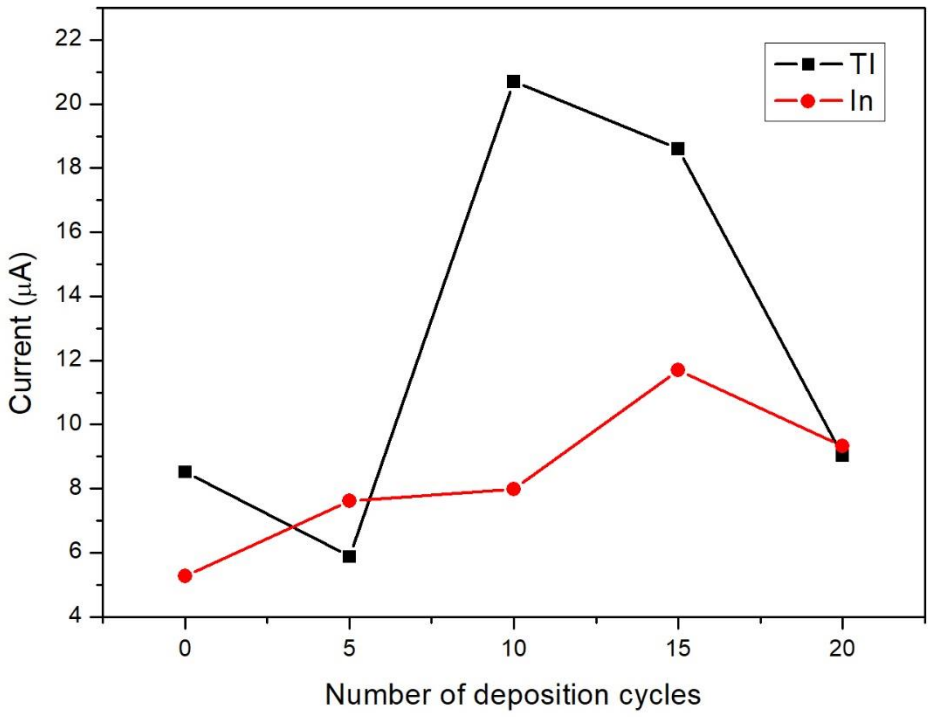

Figure 5. 3: Effect of number of cycles on the stripping peak currents of TI^{1+} and In^{3+} at the ERGO-CPE in 0.1 M acetate buffer (pH 4.6) at 30 s deposition time

5.5 Effect of Electrochemically-reduced Graphene oxide CPEs

The peak current responses of the unmodified CPE and ERGO-CPE towards TI^{1+} and In^{3+} in 0.1 M acetate buffer (pH 4.6) are compared in Figure 5.4. An enhanced peak is observed for TI^{1+} and In^{3+} at the ERGO-CPE in comparison to the unmodified CPE, indicating improved sensitivity towards the heavy metal ions. The higher surface area-to-volume ratio, enhanced electron transfer rates and conductivity owing to quantum confinement of ERGO in the nanometre range (1-100 nm) all contribute towards the improvement in stripping peak current [74]. The oxidation potentials of TI^{1+} and In^{3+} appear at -0.78 and -0.65 V, respectively due to being re-oxidized during the stripping step [74, 13] and result from the redox reactions (Equations 5.1 and 5.2) [13].

Equation 5. 1 $Mn^{n+} + ne^- \rightarrow M$ *(deposition step) (reduction step)*

Equation 5. 2 $M \rightarrow Mn^{n+} + ne^-$ *(stripping step) (oxidation step)*

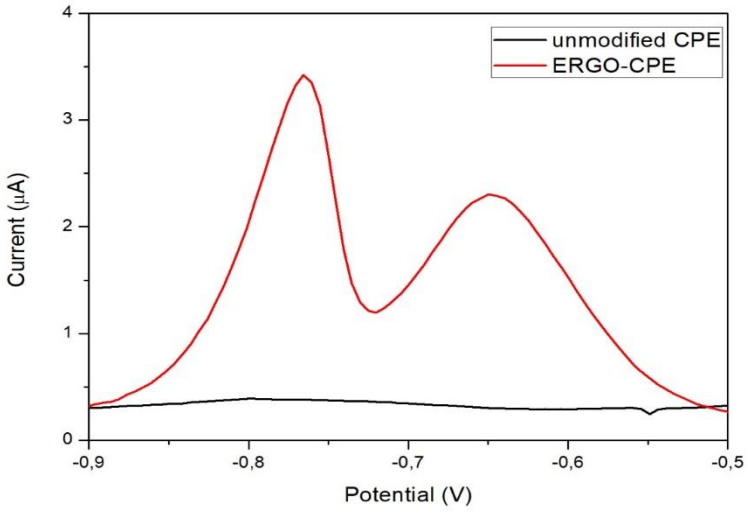

Figure 5. 4: SWASV of 20 μg L^{-1} TI^{1+} and In^{3+} at unmodified CPE and ERGO-CPE. Supporting electrolyte: 0.1 M acetate buffer (pH 4.6), amplitude (0.02 V), frequency (50 Hz), deposition time (120 s), deposition potential (-1.4 V) and rotation speed (1000 rpm).

5.6 Optimization of Instrumental parameters

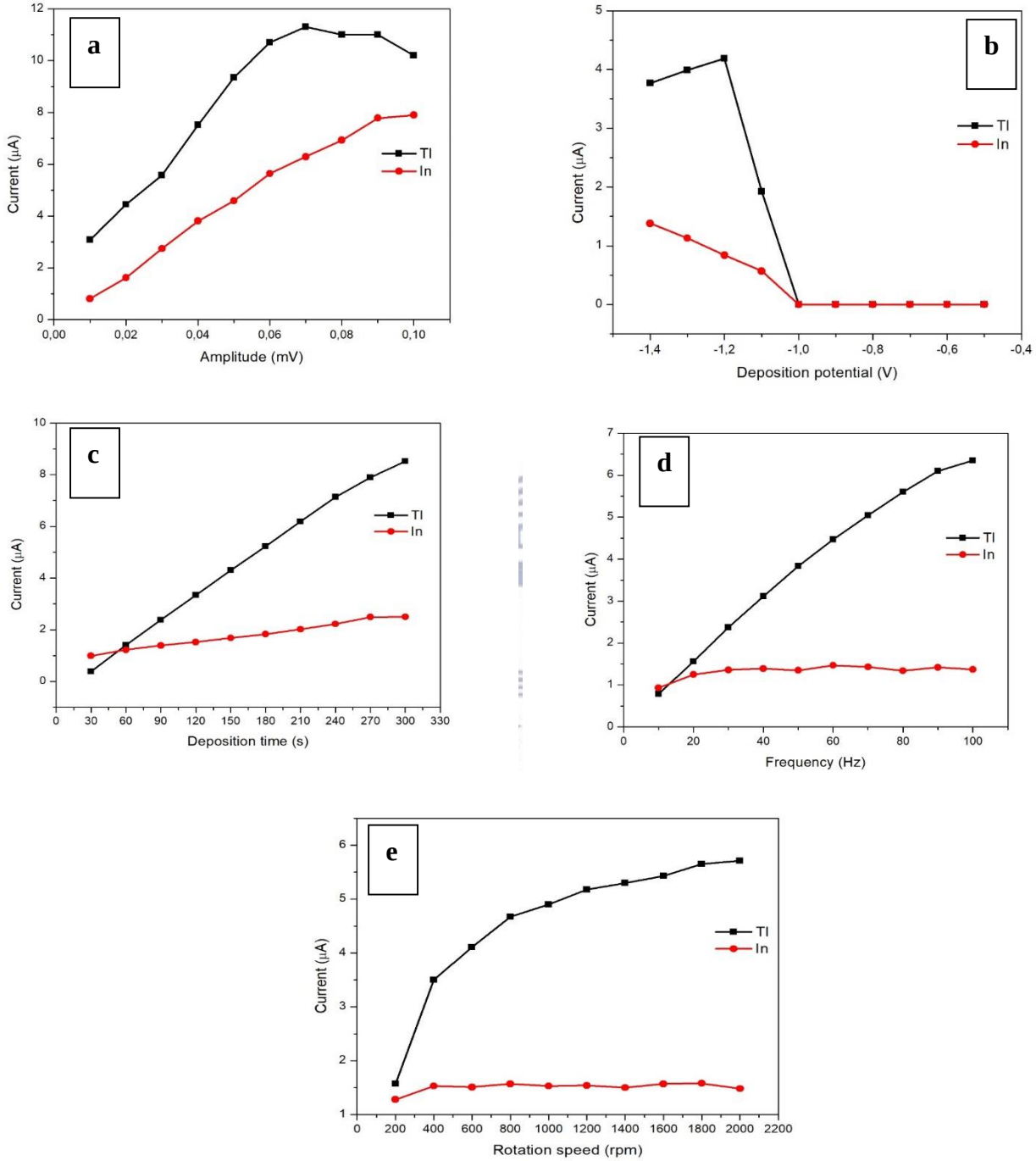

Figure 5. 5: The effect of (a) amplitude, (b) deposition potential, (c) deposition time, (d) frequency and (e) rotation speed on the peak currents of 30 μg L^{-1} of Tl^{1+} and In^{3+} at the ERGO-CPE in supporting electrolyte (0.1 M acetate buffer, pH 4.6).

The square wave parameters affecting the analytical response at the ERGO-CPE are the amplitude, deposition potential, deposition time, frequency and rotation speed and their effect are shown in Figure 5.5.

The influence of amplitude was investigated on the peak currents of TI^{1+} and In^{3+} in the potential range from 0.01 to 0.1 V in Figure 5.5a. The peak currents for TI^{1+} increases as the amplitude increases from 0.01 to 0.07 V, however the peak currents decreased from 0.08 to 0.1 V. The peak currents for In^{3+} increases as the amplitude increases. An optimum of 0.02 V for amplitude was chosen due to no significant increase in peak current with further amplitude increase.

The influence of deposition potential on the peak currents of TI^{1+} and In^{3+} at the ERGO-CPE was studied in the potential range from +0.3 to -1.4 V in Figure 5.5b. At potentials more positive than the oxidation potentials of individual metal ions no stripping peaks were observed at -1.0 V for TI^{1+} and In^{3+} due to the suppression of the reduction reaction responsible for the deposition of metal ions from solution onto the electrode surface. The peak currents for TI^{1+} increases from -1.4 to -1.2 V, due to the preferential reduction and deposition of metal ions at the electrode surface [74, 6], whereas a decrease in peak currents attributes to electrode saturation which is observed for In^{3+} from -1.3 V. A potential of -1.4 V was selected for the optimum.

The deposition time on the peak currents for TI^{1+} and In^{3+} is shown in Figure 5.5c. As the deposition time increased between 30-300 s, the peak currents increased. This is due to more time allowed for the reduction and deposition to occur at the electrode surface [13], [74]. A deposition time of 120 s was chosen for further analysis.

The effect of frequency on the peak currents of TI^{1+} and In^{3+} at the ERGO-CPE was examined in the potential range from 10 to 100 Hz in Figure 5.5d. The peak current for TI^{1+} increased with increasing frequency and is attributed to the increase in scan rate with increasing

frequency, however for In^{3+} it remains more or less constant. A frequency of 50 Hz was chosen as the optimum.

The rotation speed allows for thorough dispersion of the bulk analyte to the electrode surface where reduction occurs. The effect of rotation speed on the peak currents of TI^{1+} and In^{3+} at the ERGO-CPE was studied from 200-2000 rpm in Figure 5.5e. As the square root of the rotation speed increased, the peak currents of TI^{1+} increased. The effect of rotation speed for In^{3+} did not have a significant change in peak currents. A rotation speed of 1000 rpm was selected as the optimum.

5.7 Analytical performance of the electrochemically reduced graphene oxide modified carbon paste electrode (ERGO-CPE)

The analytical performance of ERGO-CPE were investigated by individual and simultaneous analysis of TI^{1+} and In^{3+} over a (5-50 μg L^{-1}) concentration range at Figure 5.6. A slight shift in the peak potentials towards more positive potentials was observed for both metal ions due to the IR-drop effect since the oxidation of the metals became less reversible [13]. Three replicate SWASV measurements were performed for each calibration range. Calibration plots constructed from data obtained from voltammograms were used to calculate the detection limits and are presented in Table 5.1. From the calibration curves in Figure 5.6, the detection limits of the metal ions were determined based on three times the standard deviation of the blank divided by the slope of the calibration curve. The standard deviation of the blank was calculated from ten replications. The detection limits and correlation coefficients for the individual analysis are shown in Table 5.1.

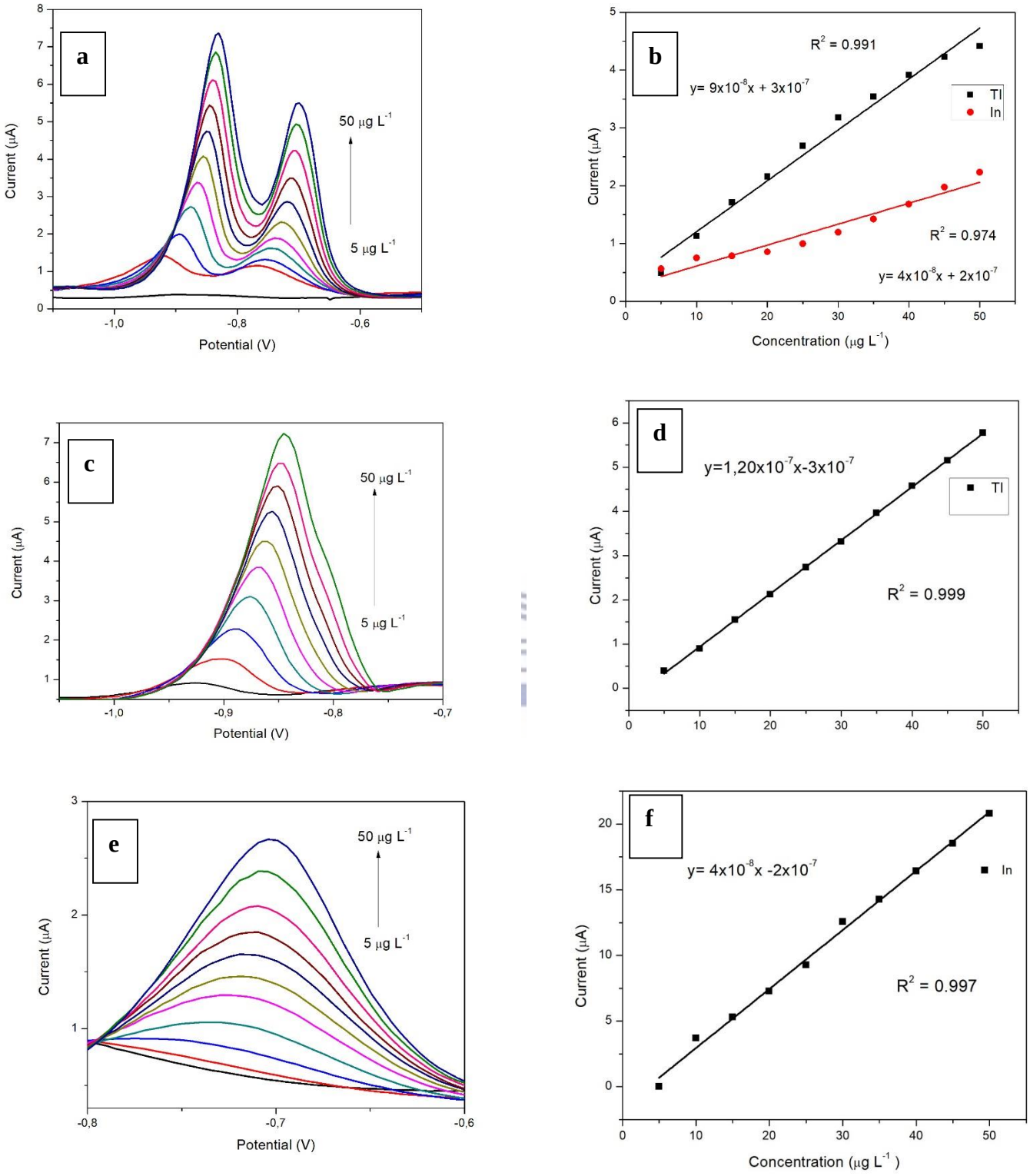

Figure 5. 6: SWASV and calibration plots for simultaneous analysis of TI and In (a and b), TI (c and d) and In (e and f) at ERGO-CPE over 5-50 µg L^{-1} for individual analysis. Supporting electrolyte (0.1 M acetate buffer, pH 4.6), deposition time (120 s), deposition potential (-1.4 V), rotation speed (1000 rpm), frequency (50 Hz), amplitude (0.02 V).

Table 5. 1: Detection limits and correlation coefficients for individual and simultaneous analysis

Individual analysis		
Analytical parameter	TI^{1+}	In^{3+}
Sensitivity (μA L μg $^{-1}$)	$1.2x10^{-7}$	$4x10^{-8}$
Standard deviation of blanks (A)	$3.9x10^{-8}$	$1.57x10^{-7}$
Detection limit (μg L^{-1})	0.975	1.04
Correlation coefficient (R^2)	0.999	0.997
Simultaneous analysis		
Analytical parameter	TI	In
Sensitivity (μA L μg L^{-1})	$9x10^{-8}$	$4x10^{-8}$
Standard deviation of blanks (A)	$3.89x10^{-8}$	$8.9x10^{-8}$
Detection limit (μg L^{-1})	1.32	1.33
Correlation coefficient (R^2)	0.991	0.974

5.8 Recovery studies of ERGO-CPE

Recovery studies on test solutions of TI^{1+} and In^{3+} were investigated at ERGO-CPE by a standard addition method shown in Figure 5.7. 20 mL portions of 0.1 M acetate buffer solution were spiked with known concentrations of target metals. Individual analysis showed improved recoveries compared to the simultaneous analysis, indicating better quantitation for both metals. Recovery percentages of TI^{1+} and In^{3+} ions from test solutions spiked with 10 μg L^{-1} TI^{1+} and In^{3+} for simultaneous analysis yielded a recovery of 90% ± 1.56% and 91% ± 5% , respectively. The recovery percentages for individual analysis of TI^{1+} and In^{3+} spiked with the

same amount as for simultaneous analysis was yielded a recovery of 95% ± 1.3% and 97% ± 6.8%, respectively.

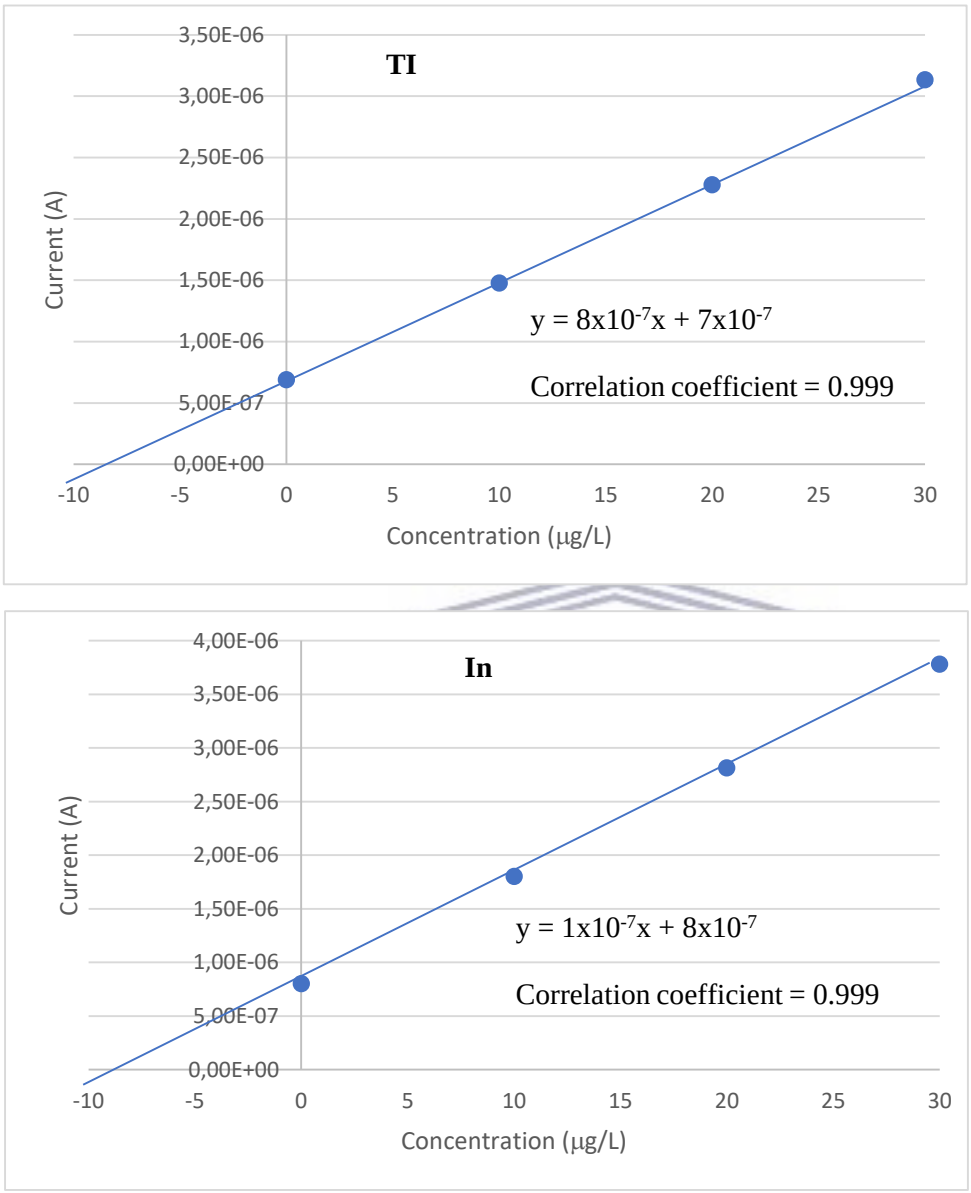

Figure 5. 7: Standard Addition plots for the individual determination (a) TI^{1+} and (b) In^{3+} at ERGO-CPE in test solutions

5.9 Application to real water samples

Tap water samples were collected in the laboratory and analyzed for TI^{1+} and In^{3+} ions using the electrochemically-reduced graphene oxide carbon paste electrode (ERGO-CPE). Individual and simultaneous analysis was performed. The amount of metal ions present in the water samples were quantified by the standard additions method. None of the heavy metal ions were detected in the original tap water samples when using a deposition potential of 120 seconds suggesting that the concentration of the metal ions was below their detection limits. Recovery percentages of TI^{1+} and In^{3+} ions from test solutions spiked with 10 μg L^{-1} TI^{1+} and In^{3+} for simultaneous analysis yielded a recovery of 90% ± 1.6% and 100% ± 8.9% , respectively. The recovery percentages for individual analysis of TI^{1+} and In^{3+} spiked with the same amount as for simultaneous analysis yielded a recovery of 95% ± 2% and 97% ± 7%, respectively. These recoveries show that ERGO-CPE with square wave anodic stripping voltammetry is suitable for monitoring TI^{1+} and In^{3+} in drinking water.

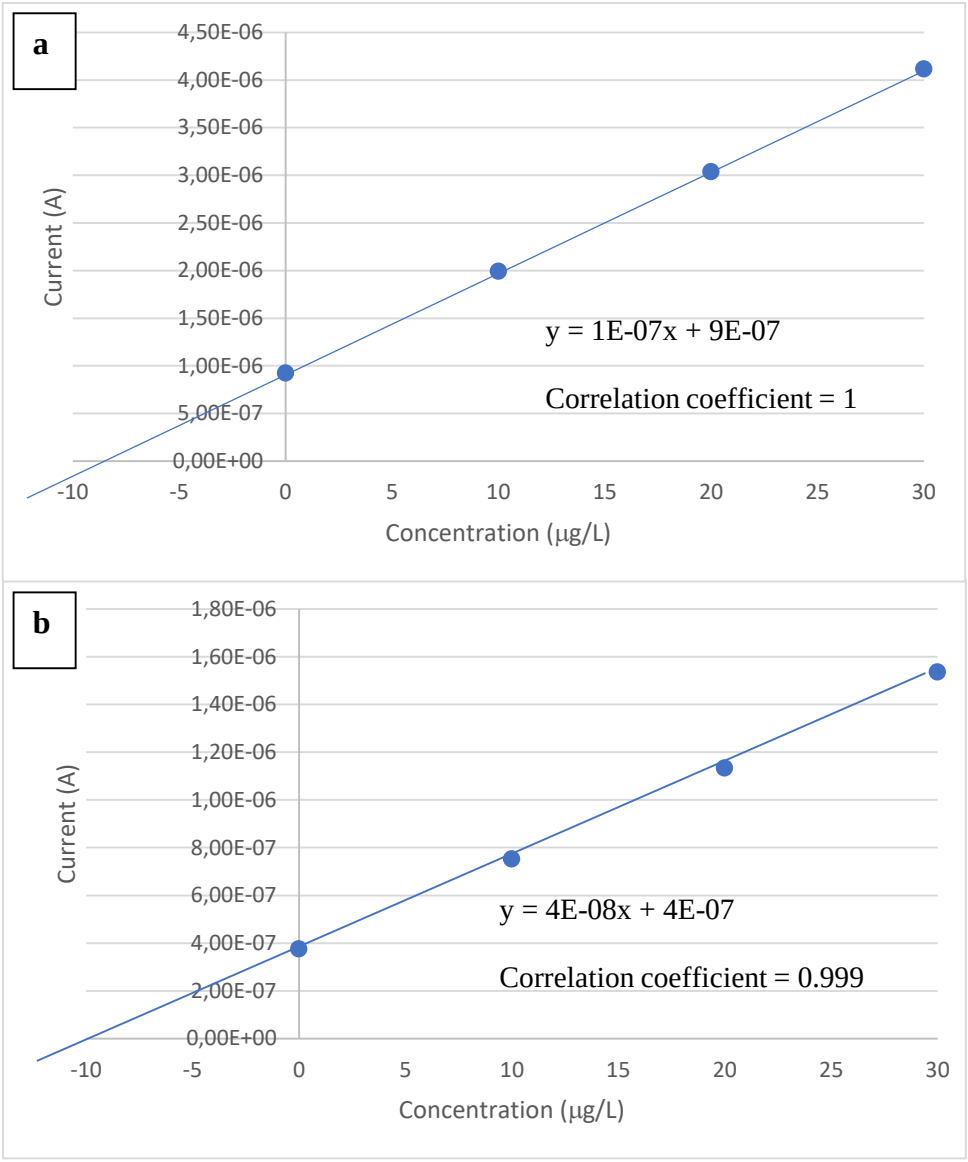

Figure 5. 8: Standard Addition plots for the simultaneous determination (a) TI^{1+} and (b) In^{3+} at ERGO-CPE in real water solutions

5.10 Interference studies

The possible interference of Zn^{2+}, Cd^{2+}, Co^{2+}, Pb^{2+} and Cu^{2+} on the anodic stripping peak of TI^{1+} was investigated individually by the addition of the interfering metal ions between 5-50 μg L^{-1} to a solution containing 5 μg L^{-1} of TI^{1+} under optimized conditions shown in Figure 5.9. Metal ions interfere with the stripping peak by producing reduction peaks that overlap with or even completely suppress the TI^{1+} peak altogether. Zn^{2+}, Co^{2+}, Pb^{2+} and Cu^{2+} did not affect the stripping peaks of TI^{1+}. However, upon the addition of Cd^{2+} caused the stripping peak of TI^{1+} to split due to the oxidation peak potential of Cd at -0.65 V, also the appearance of Zn^{2+} at -1.1 V was present. Possible explanation was due to contamination.

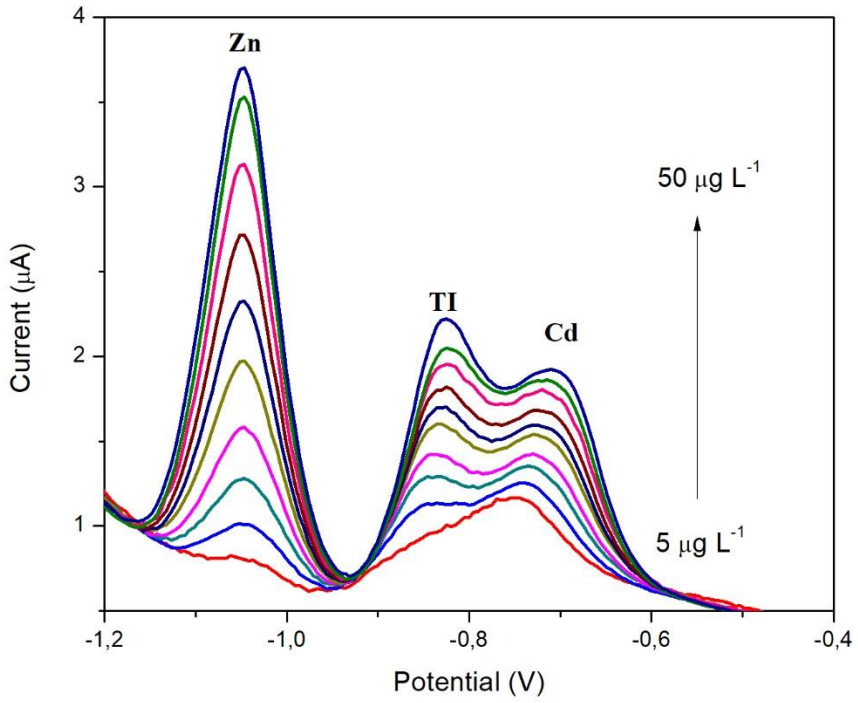

Figure 5. 9: Interference plot for TI^{1+} in the presence of Cd^{2+} in the range (5-50 μg L^{-1}) at ERGO-CPE. Supporting electrolyte (0.1 M acetate buffer, pH 4.6), deposition time (120 s), deposition potential (-1.4 V), rotation speed (1000 rpm), frequency (50 Hz), amplitude (0.02 V)

5.11 Conclusions

The electrochemically-reduced graphene oxide modified carbon paste electrode (ERGO-CPE) resulted in a sensitive sensing platform for the detection of TI^{1+} and In^{3+} by square wave anodic stripping voltammetry. Improved detection limits were achieved compared to previous reported literature in drinking water due to electron transfer rate and surface area to volume ratio due to the graphene oxide. The analytical application of the ERGO-CPE was assessed by recovery studies and real sample analysis within a 10% error.

Chapter Six:

Electrochemically-reduced Graphene Oxide Carbon Paste Mercury film electrodes (ERGO-CP-HgE)

6.1 Introduction

In this chapter the use of SWASV together with an *in situ* mercury film at an electrochemically-reduced carbon paste electrode was investigated for the detection of TI^{1+} and In^{3+} in water samples.

6.2 Influence of the number of electrodeposition cycles

Figure 6.1 shows that the amount of electrochemical reduction cycles have an effect on the stripping peak currents of TI^{1+} and In^{3+}. An increase is observed for TI^{1+} up to 10 cycles and then decreases at 15 and 20 cycles, whereas for In^{3+} it increases at 15 cycles and decreases at 20 cycles. A deposition of 10 cycles was selected for TI^{1+} and 15 cycles was selected for In^{3+} as the optimum number of cycles for the detection of heavy metal ions at the ERGO-CP-HgE.

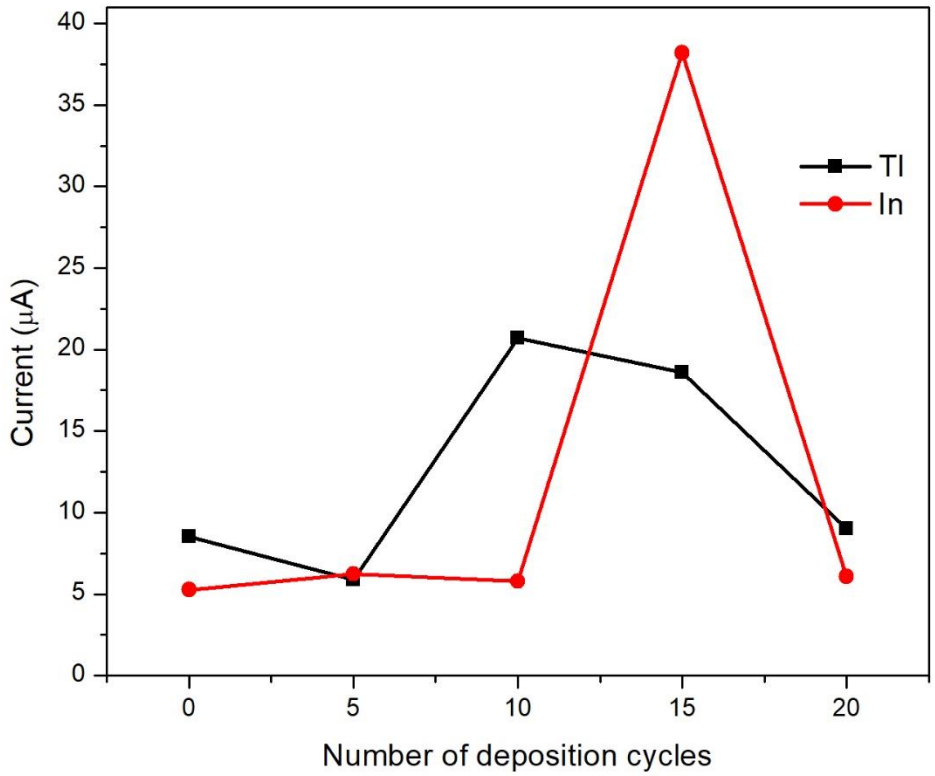

Figure 6. 1: Effect of number of cycles on the stripping peak currents of Tl^{1+} and In^{3+} at the ERGO-CP-HgE in 0.1 M acetate buffer (pH 4.6) at 30 s deposition time

6.3 Effect of Electricochemically-reduced Graphene oxide modified CPEs

The peak current responses of the unmodified CPE and ERGO-CP-HgE towards TI^{1+} and In^{3+} in 0.1 M acetate buffer (pH 4.6) for individual analysis are compared in Figure 6.2 (a and b), respectively An enhanced peak is observed for both TI^{1+} and In^{3+} at the ERGO-CP-HgE in comparison to the unmodified CPE. The oxidation potentials of the metal ions appear at -0.85 V and -0.65 V, respectively for TI^{1+} and In^{3+} and result from the redox reactions (equations 6.1 and 6.2). Simultaneous analysis was not possible due to the positive shift of the peak current of Thallium in the presence of mercury, which resulted in a merged peak rather than two separate peaks which is shown in Figure 6.3. Due to this, no further simultaneous analysis was carried out in this research.

Equation 6. 1 $Mn^{n+} + ne^- + Hg^{2+} \rightarrow M(Hg)$ (deposition step) (reduction reaction)

Equation 6. 2 $M(Hg) \rightarrow Mn^{n+} + ne^- + Hg^{2+}$ (stripping step) (oxidation reaction)

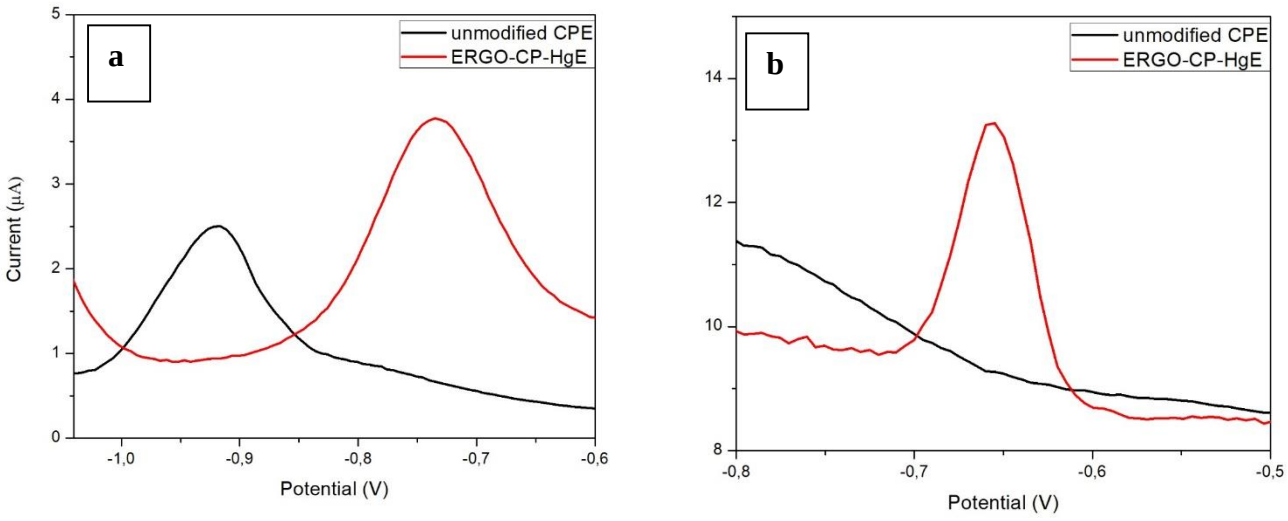

Figure 6. 2: SWASV of 30 μg L^{-1} (a) TI^{1+} and (b) In^{3+} at unmodified CPE and ERGO-CP-HgE .Supporting electrolyte: 0.1 M acetate buffer (pH 4.6), amplitude (0.02 V), frequency (50 Hz), deposition time (120 s), deposition potential (-1.3 V) and rotation speed (1000 rpm).

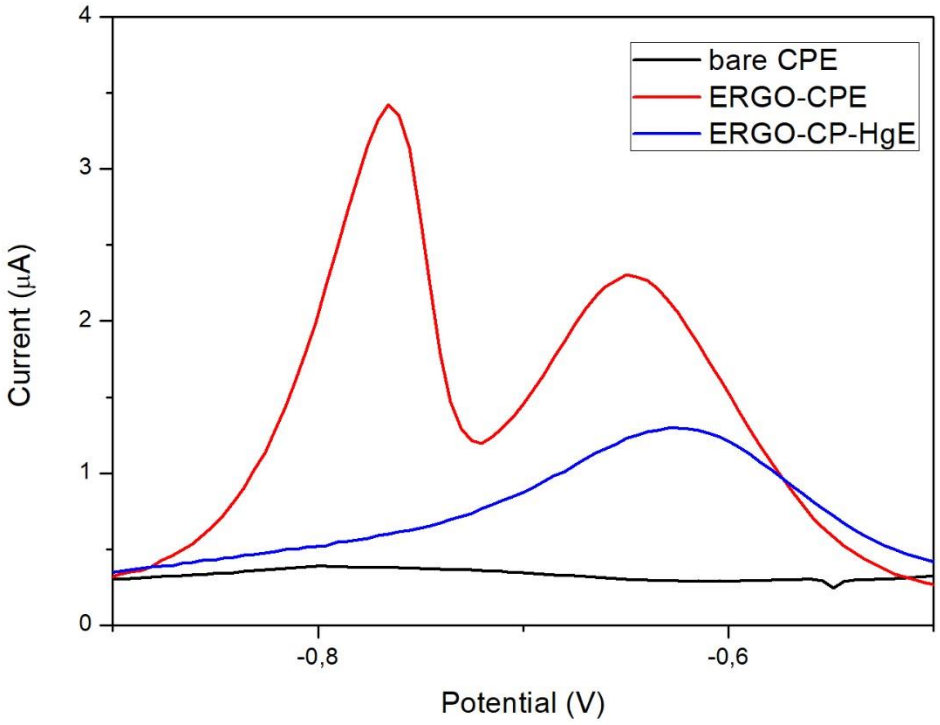

Figure 6. 3: SWASV of 20 μg L^{-1} Tl^{1+} and In^{3+} at bare CPE, ERGO-CPE and ERGO-CP-HgE .Supporting electrolyte: 0.1 M acetate buffer (pH 4.6), amplitude (0.02 V), frequency (50 Hz), deposition time (120 s), deposition potential (-1.3 V) and rotation speed (1000 rpm).

6.4 Effect of the mercury ion (Hg^{2+}) concentration

The influence of the mercury ion concentration leading to mercury film formation at the surface of the unmodified CPE was studied in a 0.1 M acetate buffer solution (pH 4.6) containing 30 µg L^{-1} each of Tl^{1+} and In^{3+}. The stripping peak currents in Figure 6.4 shows an increase for In^{3+} as the Hg^{2+} ion concentration increased from 500 – 5000 µg L^{-1} . For In^{3+} the concentration of Hg film is directly proportional to the thickness of the Hg film [13]. However, for Tl^{1+} the stripping peak currents do not increase but maintain a plateau with increasing Hg^{2+} ion concentration. Due to this behaviour, the mercury concentration of 500 µg L^{-1} for Tl^{1+} and 2000 µg L^{-1} for In^{3+} was chosen.

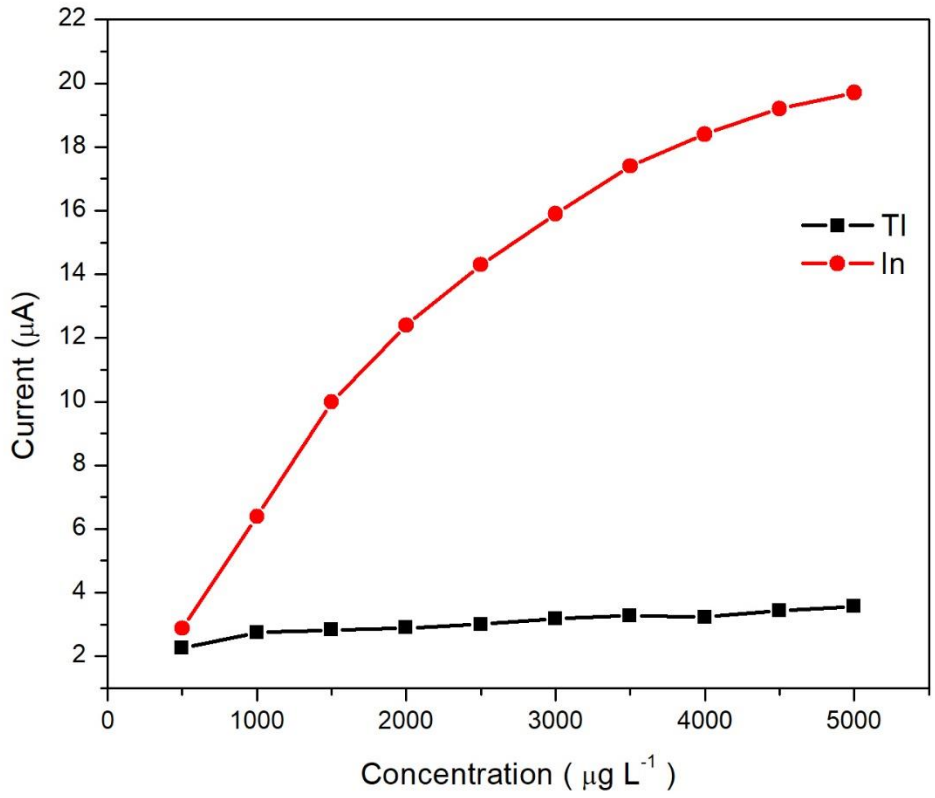

Figure 6. 4: Effect of mercury ion concentration on the stripping peak current of Tl^{1+} and In^{3+} at electrochemically reduced graphene oxide carbon paste mercury film electrode (ERGO-CP-HgE) in a 0.1 M acetate buffer solution (pH 4.6) containing 30 µg L^{-1} of each metal

6.5 Optimisation of Instrumental parameters

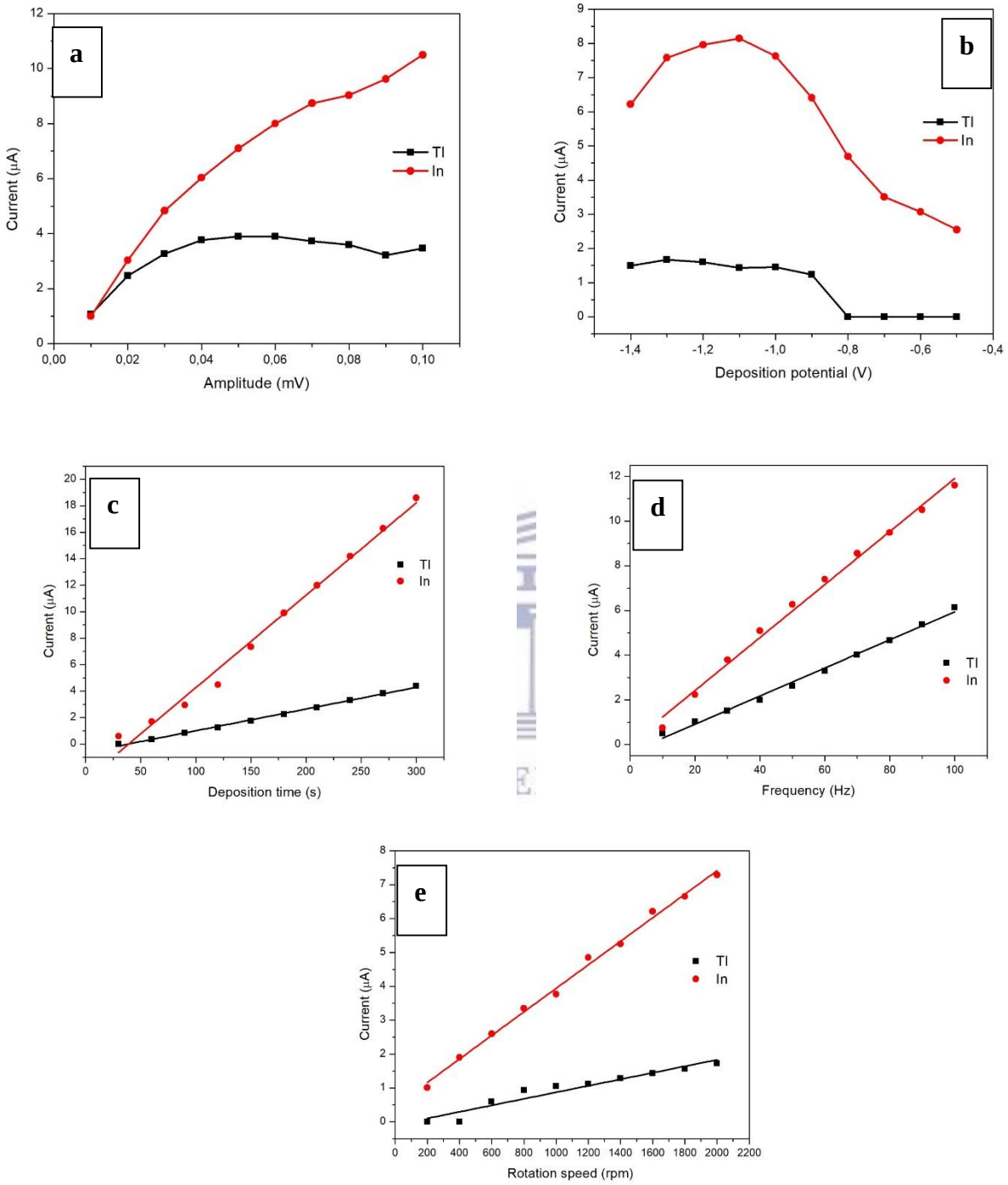

Figure 6. 5: The effect of (a) amplitude, (b) deposition potential, (c) deposition time, (d) frequency and (e) rotation speed on the peak currents of 30 µg L^{-1} of Tl^{1+} and In^{3+} at the ERGO-CP-HgE in supporting electrolyte (0.1 M acetate buffer, pH 4.6)

The influence of amplitude was investigated on the peak currents of TI^{1+} and In^{3+} in the potential range from 0.01 to 0.1 V in Figure 6.5a. As the amplitude increased from 0.01 to 0.05 V, the peak currents for both metals plateaus. An optimum of 0.02 V for amplitude was chosen.

The influence of deposition potential on the peak currents of TI^{1+} and In^{3+} at the ERGO-CP-HgE was studied in the potential range from -0.3 to -1.4 V in Figure 6.5b. The peak current for TI^{1+} gradually plateaus at -1.4 to -0.9 V and decreases from -0.8 to -0.5 V, whereas the peak currents for In^{3+} increases till -1.0 V and gradually decreases from -1.0V onwards. A potential of -1.3V was selected for the optimum for both metals.

The deposition time on the peak currents for TI^{1+} and In^{3+} is shown in Figure 6.5c. As the deposition time increased between 30-300 s, the peak currents increased. This is due to more time allowed for the reduction and deposition to occur at the electrode surface [74]. A deposition time of 120 s was chosen for further analysis for both metals.

The effect of frequency on the peak currents of TI^{1+} and In^{3+} at the ERGO-CP-HgE was examined in the potential range from 10 to 100 Hz in Figure 6.5d. The peak current for TI^{1+} and In^{3+} increased linearly. An increase in the frequency results in an increase of the scan rate. A frequency of 50 Hz was chosen as the optimum.

The effect of rotation speed on the peak currents of TI^{1+} and In^{3+} at the ERGO-CP-HgE was studied from 200-2000 rpm in Figure 6.5e. As the square root of the rotation speed increased, the peak currents of the metals increased. The rotation speed allows for thorough dispersion of the bulk analyte to the electrode surface where reduction occurs [74]. A rotation speed of 1000 rpm was selected as the optimum.

6.6 Analytical performance of the electrochemically reduced graphene oxide modified carbon paste mercury-film electrode (ERGO-CP-HgE)

The analytical performance of ERGO-CP-HgEs were investigated by individual analysis of TI^{1+} and In^{3+} over a concentration range (5-50 μg L^{-1}) . Figures 6.6 show the voltammograms and calibration plots for individual analyses. Calibration plots constructed from data obtained from voltammograms were used to calculate the detection limits and are presented in Table 6.1. From the calibration curves in Figure 6.6, the detection limits of the metal ions were determined based on three times the standard deviation of the blank divided by the slope of the calibration curve. The standard deviation of the blank was calculated from ten replications in the presence of Hg^{2+} ions. A summary of previously reported analyses for TI^{1+} and In^{3+} on various electrodes are shown in Table 6.2.

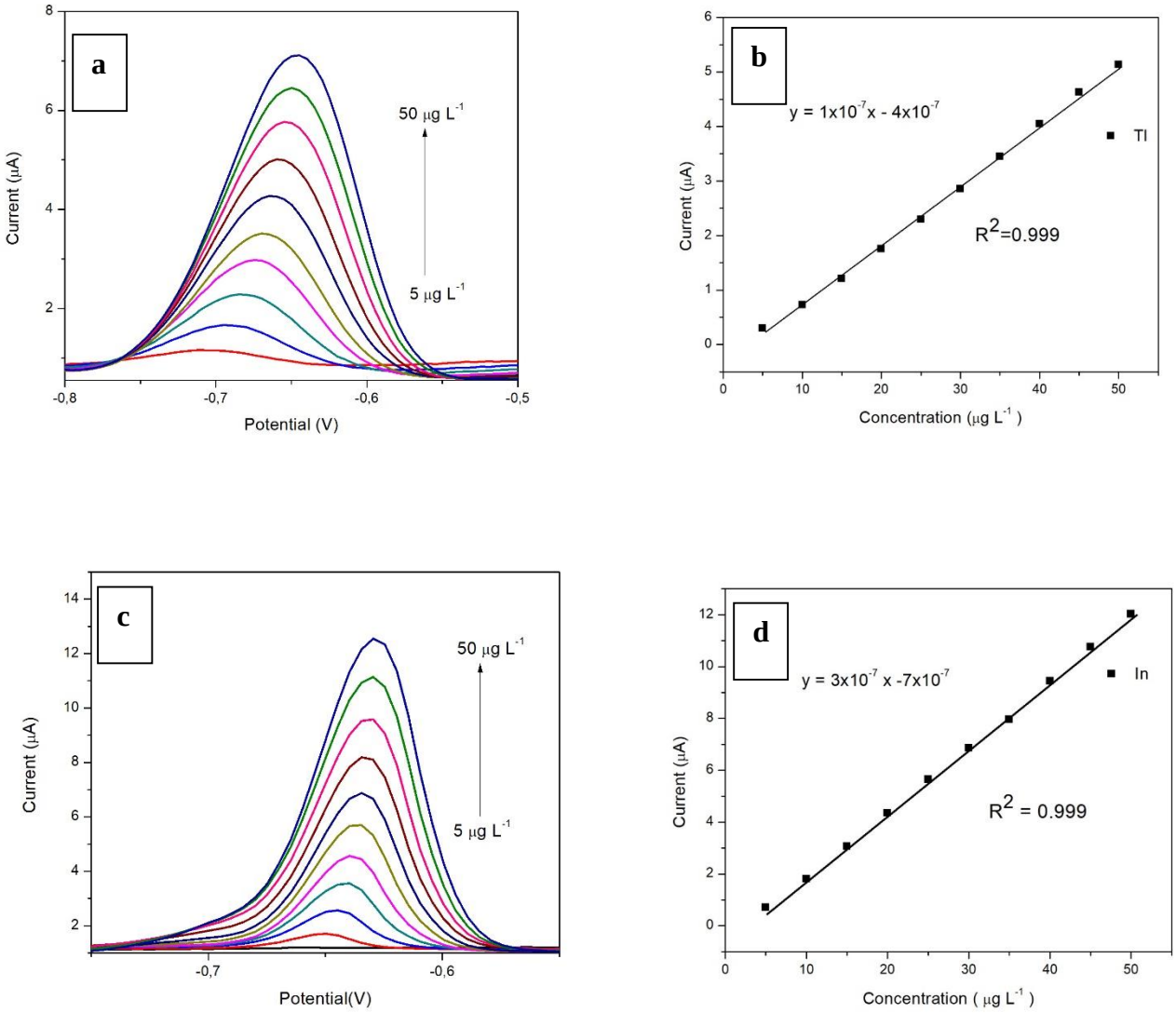

Figure 6. 6: SWASV and calibration plots for individual analysis of (a and b) TI^{1+} and (c and d) In^{3+} at ERGO-CP-HgE over 5-50 µg L^{-1}. Supporting electrolyte (0.1 M acetate buffer, pH 4.6), deposition time (120 s), deposition potential (-1.3 V), rotation speed (1000 rpm), frequency (50 Hz), amplitude (0.02 V)

Table 6. 1: Detection limits and correlation coefficient for individual analysis

Analytical parameter	TI^{1+}	In^{3+}
Sensitivity (μA L μg L^{-1})	$1.10x10^{-7}$	$3x10^{-7}$
Standard deviation of blanks (A)	$8.8x10^{-8}$	$9.76x10^{-8}$
Detection limit (μg L^{-1})	2.4	1.1
Correlation coefficient (R^2)	0.999	0.999

Table 6. 2: Previous reported detection limits for TI^{1+} and In^{3+} at various electrodes

Metals detected	Electrode substrate	Measurement technique	Deposition time (s)	Detection limit ($\mu g\ L^{-1}$)	Reference
Cd, Cu, Pb, Zn, TI, In	Sb-GCE	SWASV	120	Cd = 0.7 Cu = 0.5 Pb = 1.5 Zn = 3.8 TI = 1.0 In = 1.4	[21]
TI and In	Sb-CPE	SWASV	120	TI = 1.4 In = 2.4	[4]
TI and In	Bi-GCE	SWASV	120	TI = 4 In = 2	[12]
TI and In	SbFE	SWASV	120	TI = 2 In = 8	[77]
Thallium	Rotating disc BiFE	SWASV	120	TI = 20	[7]
TI and In	ERGO-CPE (individual analysis)	SWASV	120	TI = 0.975 In = 1.04	[In this work]
TI and In	ERGO-CPE (simultaneous analysis)	SWASV	120	TI = 1.32 In = 1.33	[In this work]
TI and In	ERGO-CP-HgE (individual analysis)	SWASV	120	TI = 2.4 In = 1.1	[In this work]

6.7 Recovery studies of ERGO-CP-HgE

Recovery studies on test solutions of TI^{1+} and In^{3+} were investigated at ERGO-CP-HgE by a standard addition method. 20 mL portions of 0.1 M acetate buffer solution were spiked with known concentrations of target metals. Individual analysis showed improved recoveries, indicating better quantitation for both metals. The recovery percentages for individual analysis of TI^{1+} and In^{3+} spiked with 10 μg L^{-1} yielded a recovery of 80% ± 4.5% and 80% ± 3.9%, respectively. A possible reason for the low recovery percentages achieved is the electrochemical sensor's inability to determine heavy metals simultaneously.

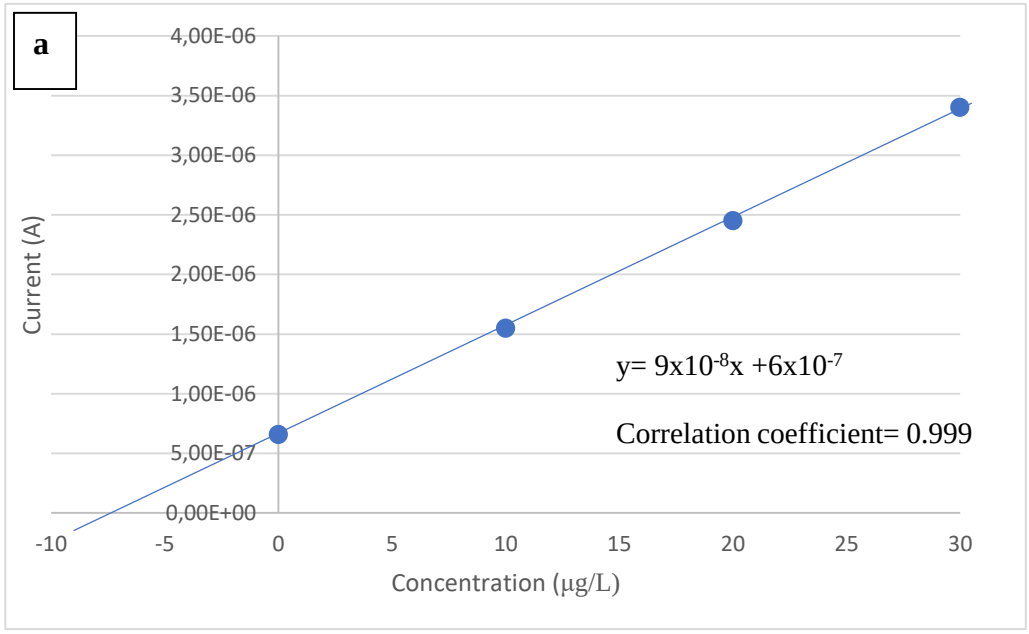

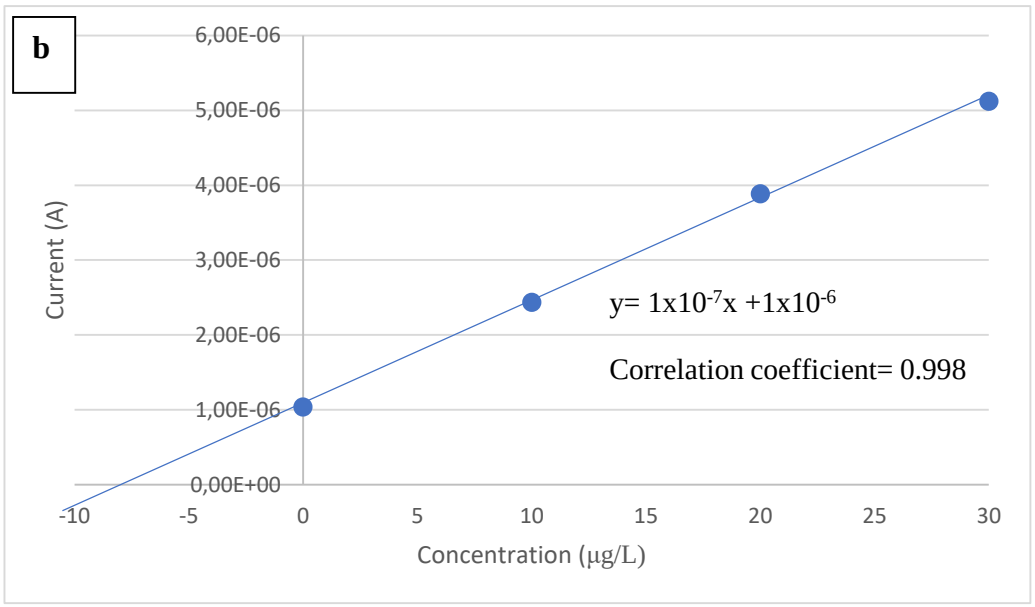

Figure 6. 7: Standard Addition plots for the individual determination (a) TI^{1+} and (b) In^{3+} at ERGO-CP-HgE in test solutions

6.8 Application to tap water samples

Tap water samples were collected in the laboratory and analysed for TI^{1+} and In^{3+} ions using the electrochemically-reduced graphene oxide modified mercury film electrode (ERGO-CP-HgE). Individual analysis was performed and the amount of metal ions present in the water samples were quantified by the standard additions method. None of the heavy metal ions were detected in the original tap water samples when using a deposition potential of 120 seconds suggesting that the concentration of the metal ions was below their detection limits. The recovery percentages for individual analysis of TI^{1+} and In^{3+} spiked with 10 μg L^{-1} yielded a recovery of 80% ± 2.2% and 90% ± 1.95%, respectively. These recoveries show that ERGO-CP-HgE with square wave anodic stripping voltammetry is suitable for monitoring TI^{1+} and In^{3+} in drinking water for individual analysis.

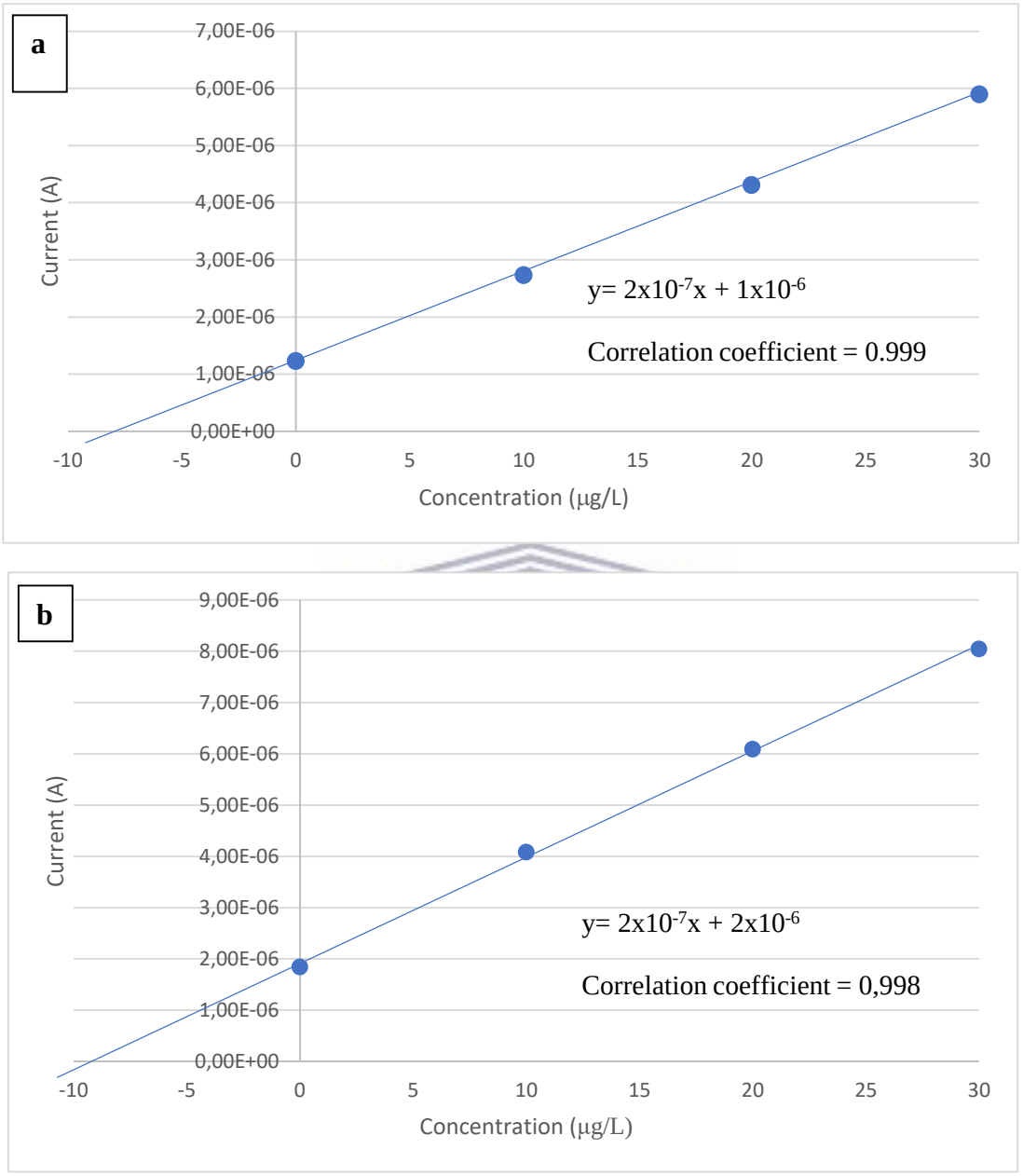

Figure 6. 8: Standard addition plots for the individual analysis of (a) TI^{1+} and (b) In^{3+} at ERGO-CP-HgE in real water samples.

6.9 Interference studies

The possible interference of Zn^{2+}, Cd^{2+}, Co^{2+}, Pb^{2+} and Cu^{2+} on the anodic stripping peak of TI^{1+} was investigated individually by the addition of the interfering metal ions between 5-50 μg L^{-1} to a solution containing 5 μg L^{-1} of TI^{1+} under optimized conditions shown in Figure 6.9. Metal ions interfere with the stripping peak by producing reduction peaks that overlap with or even completely suppress the TI^{1+} peak altogether. Zn^{2+}, Co^{2+}, Pb^{2+} and Cu^{2+} did not affect the stripping peaks of TI^{1+}. However, upon the addition of Cd^{2+} caused the stripping peak of TI^{1+} to split due to the oxidation peak potential of Cd at -0.65 V. This concludes that Cd is an interference towards TI^{1+}.

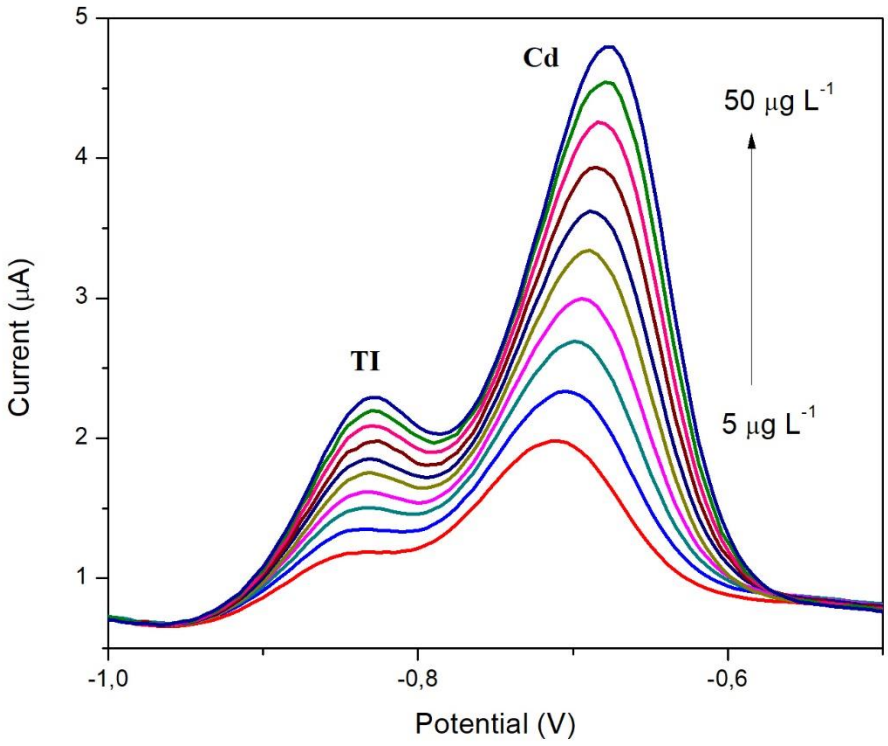

Figure 6. 9: Interference plot of TI^{1+} in the presence of Cd^{2+} in the range (5-50 μg L^{-1}). Supporting electrolyte (0.1 M acetate buffer, pH 4.6), deposition time (120 s), deposition potential (-1.3 V), rotation speed (1000 rpm), frequency (50 Hz), amplitude (0.02 V)

6.10 Conclusions

The electrodeposited graphene oxide carbon paste mercury film electrode (ERGO-CP-HgE) showed good detection limits compared to previous reported literature. The analytical application of the ERGO-CP-HgE was assessed by recovery studies and real sample analysis within a 5% error.

Chapter Seven:

Conclusions and Future Work

7.1 Conclusions

Graphene oxide was synthesized by the modified Hummer's method by oxidizing graphite to graphene oxide by $KMnO_4$ and H_2SO_4. The synthesized nanomaterial was characterized by HR-TEM, HR-SEM, FTIR, Raman and XRD.

The ERGO-CP-HgE was prepared by electro-deposition of graphene oxide onto the surface of the electrode followed by the *in-situ* deposition of mercury thin films. ERGO-CP-HgE was utilized to detect selected heavy metals namely, TI^{1+} and In^{3+}. The instrumental parameters (deposition potential, deposition time, rotation speed, frequency and amplitude) have been optimized. Hence, the deposition potential of -1.3 V, deposition time of 120 s, rotation speed of 1000 rpm, frequency of 50 Hz and amplitude of 0.02 V were identified as the optimum for the determination of the target metal ions. The detection limits using ERGO-CP-HgE for individual analysis were 2.4 and 1.1 μg L^{-1} for TI^{1+} and In^{3+} , respectively. Simultaneous analysis for TI^{1+} and In^{3+} was not obtained, due to the positive shift in the thallium peak in the presence of mercury. Hence, the simultaneous peak merges into one peak and an analysis for separate peak heights are inconclusive.

When using ERGO-CPE, the detection limits for TI^{1+} and In^{3+} were 0.975 and 1.04 μg L^{-1} for individual analysis. The detection limits for simultaneous analysis for TI^{1+} and In^{3+} were 1.32 and 1.33 μg L^{-1}, respectively.

The ERGO-CPE showed improved detection limits for TI^{1+} and In^{3+}, compared to ERGO-CP-HgE.

The application for real water sample at ERGO-CP-HgE and ERGO-CPE for the determination of the metal ions was performed by standard addition method. ERGO-CPE showed better recoveries compared to ERGO-CP-HgE .

7.2 Future work

The future work in this project will deal with:

The application of the ERGO-CPE on other real samples such as waste water or industrial waste water also, determination of other toxic heavy metals such as Pd, As, etc.

Developing a portable device using screen-printed electrodes (SPE) modified with graphene oxide for the on-site detection of heavy metal ions.

References

1. Honeychurch, K. C. Recent Developments in the Stripping Voltammetric Determination of Indium. *World J. Anal. Chem.* **1,** 8–13 (2013).

2. Jan, A. T., Azam, M., Siddiqui, K., Ali, A. & Choi, I. Heavy Metals and Human Health : Mechanistic Insight into Toxicity and Counter Defense System of Antioxidants. *Int. J. Mol. Sci.* **16,** 29592–29630 (2015).

3. Lee, G. J., Lee, H. M., Uhm, Y. R., Lee, M. K. & Rhee, C. K. Square-wave voltammetric determination of thallium using surface modified thick-film graphite electrode with Bi nanopowder. *Electrochem. commun.* **10,** 1920–1923 (2008).

4. Sopha, H. *et al.* Insights into the simultaneous chronopotentiometric stripping measurement of indium(III), thallium(I) and zinc(II) in acidic medium at the in situ prepared antimony film carbon paste electrode. *Electrochim. Acta* **55,** 7929–7933 (2010).

5. Zou, L., Zhang, Y. & Qin, H. Simultaneous Determination of Thallium and Lead on a Chemically Modified Electrode with Langmuir – Blodgett Film of a p -tert-Butylcalix [4] arene Derivative. *Electroanalysis* **21,** 2563–2568 (2009).

6. Kozina, S. A. Stripping Voltammetry of Thallium at a Film Mercury Electrode. *J. Anal. Chem.* **58,** 1067–1071 (2003).

7. Jorge, E. O., Neto, M. M. M. & Rocha, M. M. A mercury-free electrochemical sensor for the determination of thallium(I) based on the rotating-disc bismuth film electrode. *Talanta* **72,** 1392–1399 (2007).

8. Kokkinos, C., Raptis, I., Economou, A. & Speliotis, T. Disposable micro-fabricated

electrochemical bismuth sensors for the determination of Tl(I) by stripping voltammetry. *Procedia Chem.* **1,** 1039–1042 (2009).

9. Aguilar, J. C., Miguel, E. R. D. S. & Gyves, J. De. Adsorptive stripping voltammetry of In (III) in the presence of pyrogallol red in chloride-acetate media. *J. Mex. Chem. Soc.* **45,** 17–20 (2001).

10. Charalambous, A. & Economou, A. A study on the utility of bismuth-film electrodes for the determination of In(III) in the presence of Pb(II) and Cd(II) by square wave anodic stripping voltammetry. *Anal. Chim. Acta* **547,** 53–58 (2005).

11. Franke, J. P. & de Zeeuw, R. A. Differential pulse anodic stripping voltammetry as a rapid screening technique for heavy metal intoxications. *Arch. Toxicol.* **37,** 47–55 (1976).

12. Wang, J., Lu, J., Anik, Ü., Hocevar, S. B. & Ogorevc, B. Insights into the anodic stripping voltammetric behavior of bismuth film electrodes. *Anal. Chim. Acta* **434,** 29–34 (2001).

13. Pokpas, K., Jahed, N., Tovide, O., Baker, P. G. & Iwuoha, E. I. Nafion-graphene nanocomposite in situ plated bismuth-film electrodes on pencil graphite substrates for the determination of trace heavy metals by anodic stripping voltammetry. *Int. J. Electrochem. Sci.* **9,** 5092–5115 (2014).

14. Bahramipur, H. & Jalali, F. Sensitive determination of paracetamol using a graphene-modified carbon- paste electrode. *African J. Pharm. Pharmacol.* **6,** 1298–1305 (2012).

15. Smarzewska, S. & Ciesielski, W. Application of a Graphene Oxide Carbon Paste Electrode for the Determination of Lead in Rainbow Trout from Central Europe. *Food Anal. Methods* **8,** 635–642 (2015).

16. Beltagi, A. M. Utilization of a montmorillonite-Ca-modified carbon paste electrode for the stripping voltammetric determination of diflunisal in its pharmaceutical formulations and human blood. *J. Appl. Electrochem.* **39,** 2375–2384 (2009).

17. Beltagi, A. M., Ismail, I. M. & Ghoneim, M. M. Square-Wave Adsorptive Cathodic Stripping Voltammeteric Determination of Manganese (II) Using a Carbon Paste Electrode Modified with Montmorillonite Clay. *Am. J. Anal. Chem.* **4,** 197–206 (2013).

18. Devnani, H. & Satsangee, S. P. Green gold nanoparticle modified anthocyanin-based carbon paste electrode for voltammetric determination of heavy metals. *Int. J. Environ. Sci. Technol.* **12,** 1269–1282 (2015).

19. Ashrafi, A. M. & Vytřas, K. Determination of Trace Bismuth (III) by Stripping Voltammetry at Antimony-Coated Carbon Paste Electrode. *Int. J. Electrochem. Sci.* **7,** 68–76 (2012).

20. Medvecký, Ľ. & Briančin, J. Possibilities of Simultaneous Determination of Indium and Gallium in Binary InGa Alloys by Anodic Stripping Voltammetry in Acetate Buffer. *Chem. Pap.* **58,** 93–100 (2004).

21. Bobrowski, A., Putek, M. & Zarebski, J. Antimony Film Electrode Prepared In Situ in Hydrogen Potassium Tartrate in Anodic Stripping Voltammetric Trace Detection of Cd(II), Pb(II), Zn(II), Tl(I), In(III) and Cu(II). *Electroanalysis* **24,** 1071–1078 (2012).

22. DeMars, R. D. Simultaneous Determination of Tin and Indium Using Anodic Stripping Voltammetry. *Anal. Chem.* **34,** 259–262 (1962).

23. Liu, T., Lai, D. & Osterioh, J. Indium as internal standard in Square Wave Anodic Stripping Analysis of Lead in blood with microelectrode arrays. *Anal. Chem.* **69,** 3539–3543 (1997).

24. Barón-Jaimez, Jairo Alberto; Marulanda-Arévalo, José Luddey; Barba-Ortega, J. J. Electrodes friendly with the environment for detect heavy metal. *Dyna* **81,** 122–128 (2014).

25. Meepun, N., Siriket, S. & Dejmanee, S. Adsorptive stripping voltammetry for determination of cadmium in the presence of cupferron on a nafion-coated bismuth film electrode. *Int. J. Electrochem. Sci.* **7,** 10582–10591 (2012).

26. Dai, X., Nekrassova, O., Hyde, M. E. & Compton, R. G. Anodic Stripping Voltammetry of Arsenic (III) Using Gold Nanoparticle-Modified Electrodes. *Anal. Chem.* **76,** 5924–5929 (2004).

27. March, G., Nguyen, T. & Piro, B. Modified Electrodes Used for Electrochemical Detection of Metal Ions in Environmental Analysis. *Biosensors* **5,** 241–275 (2015).

28. Bott, A. Stripping Voltammetry. *Current Separations* **12,** 141–147 (1993).

29. Abollino, O., Giacomino, A., Malandrino, M., Piscionieri, G. & Mentasti, E. Determination of mercury by anodic stripping voltammetry with a gold nanoparticle-modified glassy carbon electrode. *Electroanalysis* **20,** 75–83 (2008).

30. Farghaly, O. a, Hameed, R. S. A. & Abu-Nawwas, A.-A. H. Analytical Application Using Modern Electrochemical Techniques. *Int. J. Electrochem. Sci.* **9,** 3287–3318 (2014).

31. Lucia, M., Campos, A. M. & van den Berg, C. M. G. Determination of copper complexation in sea water by cathodic stripping voltammetry and ligand competition with salicylaldoxime. *Anal. Chim. Acta* **284,** 481–496 (1994).

32. Gledhill, M. & Van den Berg, C. M. G. Determination of complexation of iron (III) with natural organic complexing ligands in seawater using cathodic stripping

voltammetry. *Mar. Chem.* **47,** 41–54 (1994).

33. Arancibia, V., Nagles, E., Gómez, M. & Rojas, C. Speciation of Cr(VI) and Cr(III) in water samples by adsorptive stripping voltammetry in the presence of pyrogallol red applying a selective accumulation potential. *Int. J. Electrochem. Sci.* **7,** 11444–11455 (2012).

34. Rojas, C., Arancibia, V., Gómez, M. & Nagles, E. Adsorptive stripping voltammetric determination of cobalt in the presence of nickel and zinc using pyrogallol red as chelating agent. *Int. J. Electrochem. Sci.* **7,** 979–990 (2012).

35. Kefala, G., Economou, A. & Voulgaropoulos, A. Adsorptive Stripping Voltammetric Determination of Trace Uranium with a Bismuth-Film Electrode Based on the U(VI)→U(V) Reduction Step of the Uranium-Cupferron Complex. *Electroanalysis* **18,** 223–230 (2006).

36. Wang, J., Lu, J., Hocevar, S. B. & Farias, P. A. M. Bismuth-Coated Carbon Electrodes for Anodic Stripping Voltammetry. *Anal. Chem.* **72,** 3218–3222 (2000).

37. Abollino, O., Giacomino, A., Ginepro, M., Malandrino, M. & Zelano, I. Analytical applications of silica-modified electrodes - A comprehensive review. *Electroanalysis* **10,** 727–734 (1998).

38. Krishnan, G. Cyclic voltammetry. 1–35 (2011).

39. Lovrić, Š. K. & Lovrić, M. Square-wave Voltammetry of Two-step Electrode Reaction. *Int. J. Electrochem. Sci* **9,** 435–444 (2014).

40. Kounaves, S. P. in *Handbook of Instrumental Techniques for Analytical Chemistry* 709–726 (1997).

41. Ferreira, M. A. & Barros, A. A. Determination of As(III) and arsenic(V) in natural

waters by cathodic stripping voltammetry at a hanging mercury drop electrode. *Anal. Chim. Acta* **459,** 151–159 (2002).

42. Batley, G. & Florence, T. Determination of Thallium in natural waters by Anodic stripping voltammetry. *Electroanal. Chem. Interfacial Electrochem.* **61,** 205–211 (1975).

43. Tang, Y., Sun, C., Yang, X., Yang, X. & Shen, R. F. Graphene Modified Glassy Carbon Electrode for Determination of Trace Aluminium(III) in Biological Samples. *Int. J. Electrochem. Sci* **8,** 4194–4205 (2013).

44. Pauliukaite, R. *et al.* Carbon paste electrodes modified with Bi2O3 as sensors for the determination of Cd and Pb. *Anal. Bioanal. Chem.* **374,** 1155–1158 (2002).

45. Duwensee, H., Adamovski, M. & Flechsig, G. U. Adsorptive stripping voltammetric detection of daunomycin at mercury and bismuth alloy electrodes. *Int. J. Electrochem. Sci.* **2,** 498–507 (2007).

46. Hezard, T. *et al.* Gold nanoparticles electrodeposited on glassy carbon using cyclic voltammetry : Application to Hg (II) trace analysis. *J. Electroanal. Chem.* **664,** 46–52 (2012).

47. Melak, F., Redi, M., Tessema, M. & Alemayehu, E. Electrochemical determination of catechol in tea samples using anthraquinone modified carbon paste electrode. *Nat. Sci.* **5,** 888–894 (2013).

48. Fischer, E. & Van Den Berg, C. M. G. Anodic stripping voltammetry of lead and cadmium using a mercury film electrode and thiocyanate. *Anal. Chim. Acta* **385,** 273–280 (1999).

49. El-Desoky, H. S. & Ghoneim, M. M. Stripping voltammetric determination of silymarin

in formulations and human blood utilizing bare and modified carbon paste electrodes. *Talanta* **84,** 223–234 (2011).

50. Kula, P. & Navra, Z. Voltammetric copper (II) determination with a montmorillonite-modified carbon paste electrode. *Fresenius. J. Anal. Chem.* **354,** 692–695 (1996).

51. Navr, Z. & Kula, P. Determination of gold using clay modified carbon paste electrode. *Fresenius. J. Anal. Chem.* **367,** 369–372 (2000).

52. Etienne, M., Bessiere, J. & Walcarius, A. Voltammetric detection of copper (II) at a carbon paste electrode containing an organically modifed silica. *Sensors Actuators B Chem.* **76,** 531–538 (2001).

53. Sun, D., Wan, C., Li, G. & Wu, K. Electrochemical determination of lead(II) using a montmorillonite calcium-modified carbon paste electrode. *Microchim. Acta* **158,** 255–260 (2007).

54. Huang, W., Yang, C. & Zhang, S. Anodic stripping voltammetric determination of mercury by use of a sodium montmorillonite-modified carbon-paste electrode. *Anal. Bioanal. Chem.* **374,** 998–1001 (2002).

55. Aglan, R. F., Mohamed, G. G. & Mohamed, H. A. Chemically modified carbon paste electrode for determination of cesium ion by potentiometric method. *Am. J. Anal. Chem.* **3,** 576–586 (2012).

56. Zhu, B. Y. *et al.* Graphene and Graphene Oxide : Synthesis , Properties , and Applications. *Adv. Mater.* **22,** 3906–3924 (2010).

57. Pop, E., Varshney, V. & Roy, A. K. Thermal properties of graphene : Fundamentals and applications. *Mater. Res. Soc.* **37,** 1273–1281 (2012).

58. Wei, D. *et al.* Synthesis of N-Doped Graphene by Chemical Vapor Deposition and Its

Electrical Properties. *Nano Lett.* **9,** 1752–1758 (2009).

59. Alam, S. N., Sharma, N. & Kumar, L. Synthesis of Graphene Oxide (GO) by Modified Hummers Method and Its Thermal Reduction to Obtain Reduced Graphene Oxide (rGO) *. *Graphene* **6,** 1–18 (2017).

60. Yin, P. T., Shah, S., Chhowalla, M. & Lee, K. Design , Synthesis , and Characterization of Graphene − Nanoparticle Hybrid Materials for Bioapplications. *Chem. Rev.* **4,** 1–49 (2014).

61. Paulchamy, B., Arthi, G. & Bd, L. A Simple Approach to Stepwise Synthesis of Graphene Oxide. *Nanomedicine Nanotechnol.* **6,** 2–5 (2015).

62. Zheng, Q. & Kim, J. in *Graphene for Transparent Conductors* 29–38 (2015).

63. Oh, W.-C. & Zhang, F.-J. Preparation and Characterization of Graphene Oxide Reduced From a Mild Chemical Method. *Asian J. Chem.* **23,** 875–879 (2011).

64. Shalaby, A. *et al.* Structural analysis of reduced graphene oxide by transmission electron microscopy. *Bulg. Chem. Commun.* **47,** 291–295 (2015).

65. Krane, N. Preparation of Graphene. *Selected Topics in Physics : Physics of Nanoscale Carbon* 1–5 (2010).

66. Dreyer, D. R., Park, S., Bielawski, W. & Ruoff, R. S. The chemistry of graphene oxide. *Chem. Soc. Rev.* **39,** 228–240 (2010).

67. Pavoski, G. *et al.* Few Layer Reduced Graphene Oxide : Evaluation of the Best Experimental Conditions for Easy Production. *Mater. Res.* **20,** 53–61 (2017).

68. Pei, S. & Cheng, H. The reduction of graphene oxide. *Carbon N. Y.* 1–19 (2011).

69. Song, J., Wang, X. & Chang, C. Preparation and Characterization of Graphene Oxide.

J. Nanomater. **2014,** 1–6 (2014).

70. Otto, D. P. & Villiers, M. M. De. Why is the nanoscale special (or not) ? Fundamental properties and how it relates to the design of nano-enabled drug delivery systems. *Nanotechnol. Rev.* **2,** 171–199 (2013).

71. Krishnamoorthy, K., Veerapandian, M., Yun, K. & Kim, S. The chemical and structural analysis of graphene oxide with different degrees of oxidation. *Carbon N. Y.* **53,** 38–49 (2012).

72. Childres, I., Jauregui, L. A., Park, W., Cao, H. & Chen, Y. P. in 1–20 (2013).

73. Marcano, D. C. *et al.* Improved Synthesis of Graphene Oxide. *ACS Nano* **4,** 4806–4814 (2010).

74. Zbeda, S. *et al.* Few-layer Binder Free Graphene Modified Mercury Film Electrode for Trace Metal Analysis by Square Wave Anodic Stripping Voltammetry. *Int. J. Electrochem. Sci* **8,** 11125–11141 (2013).

75. Galpaya, D. Synthesis, Characterization and Applications of Graphene oxide-polymer nanocomposites. (Queensland University of Technology, 2015).

76. Jahanshahi, M., Rashidi, A. M. & Ghoreyshi, A. A. Synthesis and Characterization of Thermally-Reduced Graphene. *Iran. J. Energy Environ.* **4,** 53–59 (2013).

77. Zhang, J., Shan, Y., Ma, J. X. & Li Du, X. Simultaneous determination of Indium and Thallium ions by Anodic Stripping Voltammetry using antimony film electrode. *Sens. Lett.* **7,** 605–608 (2009).